MASTER THESIS

Variability in the equivalent permeability and qf/qm ratio as obtained from discrete fracture and matrix DFM models built from the Teapot Dome dataset

Kogler Kerstin, BSc.

Chair of Reservoir Engineering, School of Petroleum Engineering

Montan University of Leoben

21/11/2013

I dedicate this thesis to my family and my closest friends,

who support me in every step I make. Thank you!

EIDESSTATTLICHE ERKLÄRUNG

Ich erkläre an Eides statt, dass ich diese Arbeit selbstständig verfasst, andere als die angegebenen Quellen und Hilfsmittel nicht benutzt und mich auch sonst keiner unerlaubten Hilfsmittel bedient habe.

AFFIDATIV

I declare in lieu of oath, that I wrote this thesis and performed the associated research myself, using only literature cited in this volume.

-------------------------------   --
             Datum   Unterschrift

Abstract

The aim of my thesis is to examine the variances in the flow properties of stochastic realisations of fracture patterns, also with regard to model size. The importance of studies on naturally fractured reservoirs has the background that a third of the worldwide oil and gas reserves are located in such reservoirs. The accurate assessment of NFR is the key to develop a reservoir model. One problem is that there is no REV in fractured media, which is the result of the high heterogeneity of NFRs. To get a lower uncertainty it is necessary to not just include the fractures in the flow modelling process but also the rock matrix, which examines the importance of DFM modelling. To compute the permeability tensor flow based up scaling was used. My thesis focuses on the determination of equivalent permeability and their anisotropy. To analyse the uncertainty, which is induced in the stochastic generation process of the models, I generated 50 equi-probable realisations of fracture sets, followed by an analysis of randomly chosen combinations of multiple fracture sets and a cluster analysis. The model size required depends on fracture length statistics, as the model has to be bigger than the mode of the fracture size to avoid a high uncertainty. To find the smallest permissible model size, to still have an acceptable computation time in the meshing and simulation process and also to have the lowest possible error, it is necessary to make a short statistical analysis such as in my provided workflow. I also compare the flow simulation results using the commercial software FracMan by Golder Associates with extended fracture generation algorithms, implemented in a Rhinoceros 5.0 plug-in by L. Mosser (2013) called StatFrac, that honour the "forbidden-zones" around fractures. A check during the fracture set generation process is made, to assure that there are no other fractures generated in the zone of relieved stress of the fracture. Following my statistical analysis of the fracture sets and their combinations, I calculated

equivalent permeability using parallel-plate law. I used a constant matrix permeability for every model and a fracture permeability which is constant within each fracture but varies for every single fracture using a configuration file. The effects of the uncertainty, which appear while randomly generating the models using the different stochastic fracture generation algorithms, are also visible in the range of my simulation results. Furthermore the impact of the orientation of the fractures on the flow has been studied. Expectedly, fracture sets aligned with the far field fluid pressure gradient have a higher velocity than perpendicular ones. To investigate the influence of the matrix permeability on equivalent permeability and flow velocity, I carried out a sensitivity analysis. The outcome is, that the higher the matrix permeability is, the higher equivalent permeability gets. The flow velocity in the fractures increases, due to the interaction between matrix and fracture sets. The matrix contributes to the flow starting with the lowest permeability used (5 mD). Rock matrix would dominate the flow with a permeability higher than 500 mD.

Kurzfassung

Ziel meiner Diplomarbeit ist es, die Variabilität der Fließeigenschaften von stochastischen Realisierungen der Riss-Muster zu untersuchen, auch im Hinblick auf die Modellgröße. Die Wichtigkeit der Studien über natürlich gerissene Lagerstätten hat den Hintergrund, dass ein Drittel der weltweiten Öl- und Gasreserven sich in solchen Lagerstätten befinden. Die genaue Beurteilung der NFR ist der Schlüssel zur erfolgreichen Entwicklung einer Riss-Lagerstätte. Um eine niedrigere Unsicherheit zu erhalten ist es erforderlich, nicht nur die Risse selbst in die Modellierung miteinzubeziehen, sondern auch die Gesteins-Matrix, was die Bedeutung der DFM Modellierung bekräftigt. Um den Permeabilitäts Tensor zu berechnen wurde „flow based up scaling" verwendet. Ein Problem ist, dass kein REV in NFR existiert, was auf die hohe Heterogenität von Riss Lagerstätten zurückzuführen ist. Meine Arbeit konzentriert sich auf die Bestimmung der entsprechenden Permeabilität und ihre Anisotropie. Um die Unsicherheit zu analysieren, die im stochastischen Generierungsprozess der Modelle herbeigeführt wird, wurden 50 gleichwahrscheinliche Realisierungen der Riss-Sets erstellt, gefolgt von einer Analyse der zufällig gewählten Kombinationen aus mehreren Rissen und eine „Cluster" - Analyse. Die mindesterforderliche Modellgröße hängt von der Riss-Längen Statistik ab. Das Modell muss größer als der häufigste Wert des größten Risses sein um hohe Varianz der Flusseigenschaften zu vermeiden. Um die geringste zulässige Modellgröße zu finden, die eine akzeptable Rechenzeit beim „Meshen" und während der Simulation mit sich bringt und die Varianz der Ergebnisse niedrig hält, ist es notwendig, eine kurze statistische Analyse wie in meinen bereitgestellten Workflow zu machen. Ein Riss-Generationsalgorithmus welcher die "verboten-Zonen" rund um Risse berücksichtigt wird ausserdem in meiner Arbeit benutzt. Eine Überprüfung

während des Riss-Generationsprozesses wird durchgeführt, um sicherzustellen, dass es keinen anderen Riss in der rundum liegenden Spannungszone Zone des bereits erstellten Risses gibt. Nach meiner statistischen Analyse der Riss Sets und deren Kombinationen kalkuliere ich die effektive Permeabilität mit dem „parallel-plate-law". Eine konstante Matrix-Permeabilität wurde für jedes Modell festgelegt und jedem Riss einzeln eine Permeabilität mithilfe einer Konfigurationsdatei zugewiesen. Welche Auswirkungen die Varianz der Modelle, die bereits im stochastischen Generierungsprozess entsteht, auch auf das „flow-based upscaling" hat wird bei der Auswertung der Ergebnisse sichtbar. In den Strömungs-Geschwindigkeitshistogrammen zeichnet sich ab, welchen Effekt die Orientierungen der Riss haben. Erwartungsgemäß, haben Risse mit die zum „far-field fluid" Druckgradient ausgerichtet sind eine höhere Geschwindigkeit als welche senkrecht dazu. Um den Einfluss der Matrix Permeabilität auf die effektive Permeabilität und Strömungsgeschwindigkeit zu untersuchen, führte ich eine Sensitivitätsanalyse durch. Das Ergebnis ist, dass je höher die Matrix-Permeabilität ist, desto höher ist die effektive Permeabilität. Die Strömungsgeschwindigkeit in den Rissen erhöht sich, aufgrund der Interaktion zwischen Matrix und Fraktur-Sets. Die Gesteinsmatrix trägt beginnend mit der am geringsten verwendeten Permeabilität von 5 mD schon zum Fluss bei. Mit einer Permeabilität höher als 500 mD würde die Matrix den Fluss dominieren.

Acknowledgements

First of all I would like to thank my supervisor, from the Chair of Reservoir Engineering at the University of Leoben, Univ.-Prof. Dipl.-Geol.PhD. Stephan Matthäi, who gave me the opportunity to work on this thesis. He always added valuable ideas to my work by looking at things from a different point of view.

Additionally, I would like to thank MSc. Caroline Milliotte. This master thesis would not have been possible without her guidance and help. She contributed to the preparation and completion of this study in many ways and was always ready to give me her valuable assistance in all regards. I also want to thank Lukas Mosser for the allowance to use his tool "StatFrac" for my thesis. Moreover I want to thank RMOTC for providing me the Teapot Dome Data set I used in my thesis. Not to forget I want to thank ITF consortium for funding my thesis. My thesis is part of the itf-ISF Phase 3 project "Improved Simulation of Faulted and Fractured Reservoirs".

Furthermore, I want to thank the whole team from the Chair of Reservoir Engineering, especially Alina Yapparova, for the great time I spent with them while writing my thesis. Last but not least I want to thank my family and my friends for their moral support.

Table of Contents

List of Figures

List of Tables

Abbreviations

API	Application Program Interface
CDF	Cumulative Distribution Function
DFM	Discrete Fracture and Matrix Model
DFN	Discrete Fracture Network
FMI	Wellbore Formation MicroImager (Log)
NFR	Natural Fractured Reservoir
NURBS	Non-Uniform Rational Basis Spline
PDF	Probability Density Function
REV	Representative Elementary Volume
STDV	Standard Deviation
qf/qm	Fracture – Matrix Flow
$k_{equ.}$	Equivalent Permeability

.

1. Introduction

The underlying reason for the considerable body of research on naturally fractured reservoirs (NFR) is probably found when considering that about a third of the worldwide oil and gas reserves are located in reservoirs of this nature. The flow properties in these reservoirs are affected by fractures in different ways. As fractured reservoirs are of highly heterogeneous and complex nature, their characterisation is more difficult and less well understood than for conventional reservoirs. Fractures can have a much higher ability to transport fluids than the rock matrix, so it is even more important to characterize them as accurate as possible. One way to study their flow properties subsequently is to stochastically generate fracture patterns from the collected geostatistical data and use these as proxy models for the NFR, whose actual geometry remains hidden in the subsurface. The key to generate stochastic fracture models is to have statistical data large enough to give a statistically acceptable representation of fracture properties (Bonnet, et al., 2001). This might be difficult as fracture geometries tend to have no homogenisation scale or REV. These models of NFRs result in different flow behaviour due to their stochastic generation (Min, et al., 2004). So, for the identic input fracture distributions, different results for e.g. equivalent permeability and qf/qm ratio can be expected.

One way for stochastic fracture modelling of NFRs is to use the DFN (Discrete Fracture Network) modelling approach. The rock matrix in DFN models is assumed to be negligible. DFN modelling is useful for homogeneous statistical data. Fracture system geometry used in DFN modelling is based on stochastic generations of fracture sets (Min, et al., 2004), so as in DFM (discrete fracture matrix) modelling. In DFM modelling

not just the flow in fractures is modelled but also in rock matrix, which reduces uncertainty of the NFR model (Bogdanov, et al., 2007). For computation of the effective permeability tensors using DFN or DFM modelling flow based upscaling is an important topic, as the chosen upscaling method can lead to a variation of effective permeability up to three orders of magnitude (Ahmed Elfeel & Geiger, 2012). The beginnings of flow calculations have been made by Snow (1969). The analogy of the flow through a fracture to a conduit of parallel plates parted by a constant aperture has been presented in his work. His assumptions are laminar flow, smooth walls and a fracture length much larger than the distance between the walls. Snow (1969) stated the cubic law, using the Navier Stokes equation for laminar single phase flow of an incompressible fluid. Using the mathematical expressions of fracture geometry with tensors published by Snow (1969), Oda (1985) published a method to analytically calculate effective permeability tensors of interconnected fractures in a computationally efficient way. As Oda (1985) just used a weighting factor to account for fracture length and has no check for fracture network connectivity, his method is limited to connective fractures with a high intensity (Ahmed Elfeel & Geiger, 2012). To also account for fracture connectivity the flow based method is used to calculate effective permeability. The equation used in this numerical method, is derived from the laws of momentum and mass. The disadvantage is that the computational expenses are higher compared to Oda's method and the results highly depend on boundary conditions (Ahmed Elfeel & Geiger, 2012). More actual research has been made by Bogdanov, et al. (2007), the work addresses the full complexity of flow in permeable fractured media, by accounting for the matrix flow and for the size polydispersivity of the fractures using a power law distribution. Two parameters have been introduced, which allow for a unified description over a wide range of fracture characteristics, including shape, fracture

density, fracture size and size dependent permeability. The first parameter is the dimensionless density which controls percolation and the second is a measure of the volumetric area of the fractures in the medium weighted by the individual permeability. Sangare, et al. (2010) determined macroscopic properties of fractured porous media governed locally by a Laplace equation. An approximation is suggested which is valid when the properties of the fluid and of the continous porous medium are not too different.

My work has a focus on flow-based upscaling with aid of discrete fracture and matrix (DFM) models. The claim of my thesis is to study the differences in the flow properties of stochastic realisations of fracture patterns. The effect of fracture arrangement, which varies due to stochastically generation of the fracture geometry, on equivalent permeability, qf/qm, percolation and so on flow velocity spectra will be discussed. The origin of the statistical data used in the modelling stem from RMOTC, the U.S. department of energy, who gave me a dataset of Teapot Dome to work with. Teapot Dome is located in central Wyoming in the southwest edge of the Powder River Basin in Natrona County, it is an asymmetric doubly plunging anticline which is basement cored. (Cooper, 2000)

In the first part of my thesis, the background of the work is introduced. I will explain the context of DFM modelling and present the origin of the geostatistical data used. Then the methodology of my work will be described. Here I start out with fracture statistics needed as input for the stochastic models. Following the stochastic fracture generation models are described. Then I come to flow based upscaling, were I present the general calculation process and the boundary conditions assumed. Before I come to the

application of my workflow the general setup and assumptions made are stated. The second part of my thesis deals with the results of my experiments on stochastically generated fracture set realizations. Results on geometrical and flow data analysis will be shown. More precisely, I studied the effect of different fracture generation algorithms used to stochastically generate fracture networks on the number of fractures, fracture intensity and fracture length distribution. The influence of the model size and the effect of the variation of matrix permeability have also been investigated. Statistical analysis methods like, probability distributions, frequency histograms, spider plots and tornado diagrams are used. To state the uncertainty the range of values are stated in giving the input value $\pm$ uncertainty. A good estimate for errors symmetrical about a value is given by the standard deviation. The workflow used in this thesis starts with the characterisation of the NFR, followed by the generation of the stochastic models. The Enhanced Baecher model (FracMan), the poisson process (StatFrac) and the random walk (StatFrac) was used to generate the stochastic models. For every stochastic model generation method I created fifty equi-probable fracture geometries. To not just study the effect of stochastic generation on fracture geometry but also the effect of a varying model size, I used three different model sizes (25, 50 and 100 meter side length).

The third part of the thesis consists of the discussion of the results, followed by the conclusion of my work, where recommendations will be presented how to deal with the uncertainty of randomly generated fracture sets.

2. Background

As already mentioned, my thesis concentrates on flow-based upscaling with the aid of DFM models. Discrete fracture and matrix modelling allows the interaction between fractures and the matrix. The rock matrix can strongly contribute to the total flow. It either contributes or dominates the total flow, depending on its permeability (Matthäi & Belayneh, 2004). This contribution, or even domination, of rock matrix and following also the interaction of fractures and matrix cannot be neglected to get results closer to reality. The correct usage of geostatistical data necessary to generate the stochastic representations of NFRs used for modelling is another important point to assess accuracy. To accuracy and the sensibility of the models I come back later in this chapter.

2.1 Origin of geostatistical data used in the modelling

The fracture data studied in this thesis were provided by RMOTC, the U.S. department of energy. The geostatistical Teapot Dome dataset I worked with just included data from one well, namely well 48-x-28, a borehole in Sandstone B layer of the Tensleep formation. The dataset contained FMI, core, reservoir, seismic and well log data. Additional data to get a statistically acceptable representative was collected using literature (Cooper, 2000; Schwartz, 2006; Lorenz & Cooper, 2011). The simplified cross-section, where all oil bearing layers are shown, is presented in Figure 1. The Tensleep formation is the deepest out of nine productive horizons and also one of the most profitable. It consists of eolian quartz-sandstone interbedded with sabkha deposits and marine dolomites (Ouenes, et al., 2010)

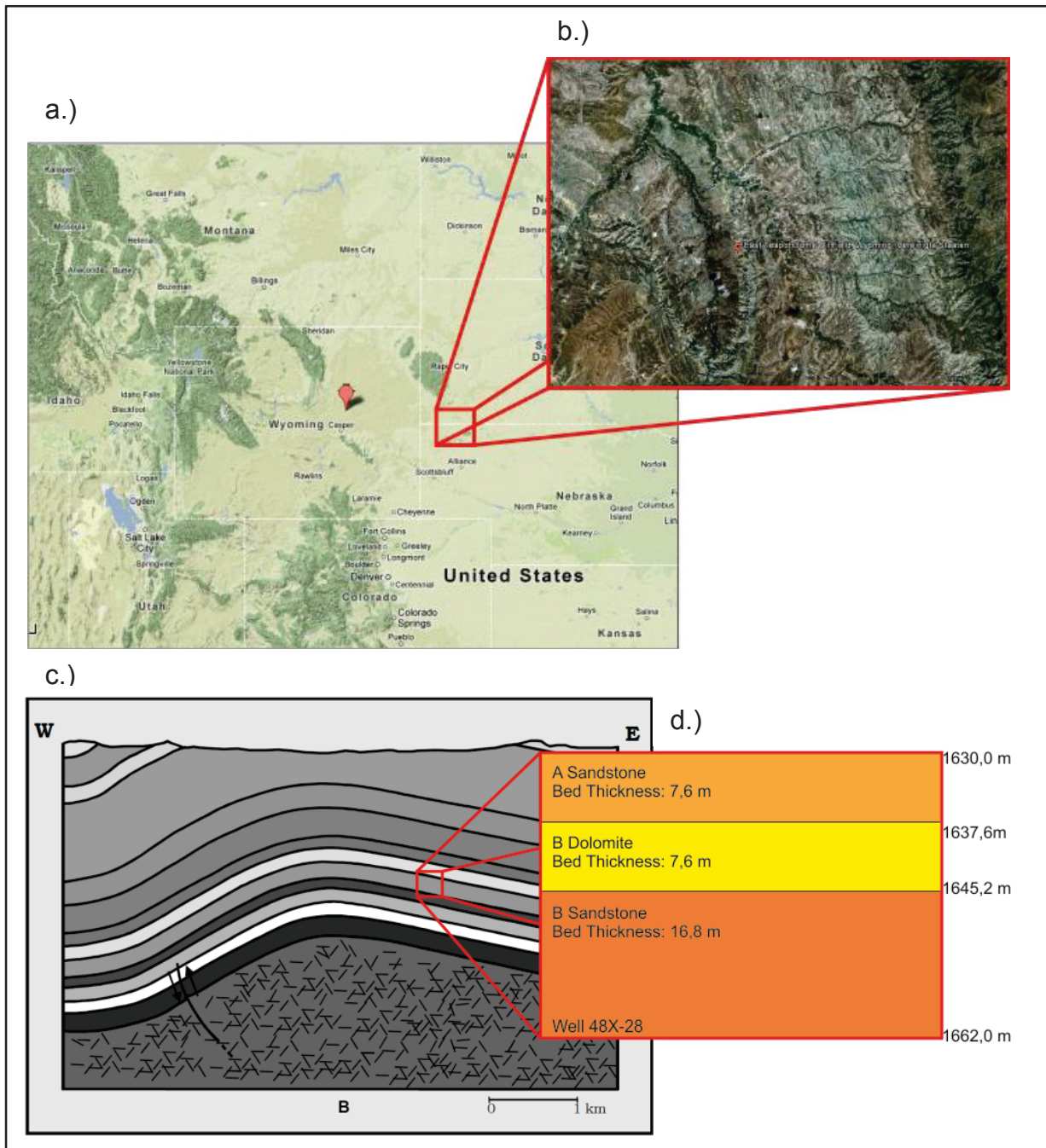**Figure 1. Teapot Dome Cross-Section**

a.)   Location of Teapot Dome in the state of Wyoming. (Inc., 2012)

b.)   Overview of the anticline structure is shown. (Inc., 2012)

c.) Cross- Section of all layers

d.) Simplified Pennsylvanian Tensleep Formation (Cooper, 2000) Sandstone B on

which this thesis focuses is found at a depth of 1645 meter for well 48-x-28 and has

a bed thickness of 16.8 meters.

3. Methodology

This section discusses the fracture characterisation using geostatistical data, algorithms used in stochastic fracture modelling, flow based upscaling and the experimental design.

3.1 Fracture statistics

Geostatistical data are necessary for fracture characterisation. Fractures form networks. A fracture network is defined as a set of individual fractures which may or may not intersect (Adler & Thovert, 1999). This network includes different fracture sets, which are defined as groups of fractures with similar orientation. In my thesis interconnected fractures are defined as a cluster. These clusters are very important as the size, geometry and spatial distribution in the model, determines if a fracture network percolates or not. A percolating fracture network has a spanning connected cluster over the length of the model. All the fractures are assumed to be open-mode fractures (Mode I), so these are no conjugate sets (Pollard & Aydin, 2007). Furthermore the fractures are presumed to be planar and circular. To define the geometry of a DFM model, the following key parameters need to be identified:

   a. *fracture orientation*

   b. *fracture intensity*

   c. *fracture spacing*

   d. *fracture size*

   e. *fracture aperture*

   a. Fracture orientation and fracture set characterization

To obtain the fracture sets, orientation data from either borehole and/or outcrop data, can be used. A sampling bias may arise, due to the difficulty in determining the

orientations of fractures parallel to the sampling line or plane (Lato, et al., 2010). Terzaghi's (1965) approach must be used to correct the orientation data. A weighting factor w is used (w=cos(x)$^{-1}$), where x is the angle between the scanline and the normal to the fracture. The mean orientation of a fracture set is used to derive the weighting factor. To get the mean orientation of the different fracture sets rose diagrams which need the input of statistically representative orientation data can be used.

b. Fracture intensity (P32)

In three dimensions fracture intensity is defined as the area of fractures in a volume. As it can't be measured directly, it is evaluated with help of P10, the fracture density. P10 is defined as the fracture frequency along a scanline of a borehole (Dershowitz, 1992). P32 is then calculated in multiplying a constant of proportionality C10 with P10. C10 depends on the orientation and size distribution of the fractures and varies between 1 and 3.

c. Fracture spacing

Fracture spacing is defined as the mean distance, measured along a perpendicular line, between fractures within a fracture set (Dershowitz, 1992). Fracture spacing is calculated with the help of P10, as it is its reciprocal.

d. Fracture size

Fracture length estimation from borehole data is usually not possible, but some bonds can be found. Schwartz (2006) calculated a fracture length distribution with help of the trace length. Bonnet et al. (2001) stated that the power law distribution is used in recent years to describe the frequency distribution of fracture properties and geometry. A power law distribution can also be used for the fracture length. It contains no characteristic length scale but an upper and lower cut-off value (Bonnet, et al., 2001).

The lower cut-off value represents the minimum fracture length. A too low value might end in high computational expenses and gives potential for discussion in terms of resolution possible and accuracy. Censoring of long fractures might also influence the accurate assessment of fracture length distribution, as these fractures might not be completely observed (Bonnet, et al., 2001).

The stochastic fracture generation algorithms in FracMan use the Pareto power-law (Equation 10) and in StatFrac a power function (Equation 11) is used to create a length distribution.

$$f(x) = \frac{b-1}{x_{min}} \left(\frac{x_{min}}{x}\right)^b \; x \geq x_{min}, \; b > 1 \qquad (10)$$

x_{min} – minimum fracture length (m)
b – coefficient (-)
x – fracture length (m)

$$f(x) = \frac{\alpha(x-a)^{\alpha-1}}{(b-a)^{\alpha}} \qquad (11)$$

α – Coefficient (m)
a – Minimum fracture length (m)
b – Maximum fracture length (m)

a. Fracture aperture

Fracture aperture is defined as the distance between the two surfaces of a fracture (Wilson & Witherspoon, 1974). To describe fracture aperture and length relationship various models are described in the literature. One is the linear elastic fracture mechanics (LEFM) model by Olson (2003). In consequence to the linear relationship between fracture aperture and length, the aspect ratio (d_{max}/L) should be constant with respect to length as it only depends on driving stress. Olson (2003) suggests this linear relationship being limited to cases of fracture mineralization under relaxed conditions or during the early, unstable stages of displacement-driven propagation. An alternative relationship which is appropriate for fractures that become mineralized while

propagating was proposed by Olson (2003). The relationship is based on LEFM, where all fractures in a population have the same stress intensity factor. The result of his sub-linear – square root – aperture to length relationship is that aspect ratio decreases with higher length of fractures as fracture aperture gets smaller with higher fracture length. Olson's method is not appropriate for closed fractures (Matthäi, 2012). Another approach would be a Mode I aperture computation from far field stress, which is similar to Olson's model and leaves the problem with closure fractures, as it might overestimates aperture due to fractures with mineral bridges (Matthäi, 2012). A method which deals correctly with closure aperture is a calculation of aperture from Joint Roughness Correlations (JRC) and empirical aperture strain curve. But this assumes having rock-type specific field data (Matthäi, 2012).
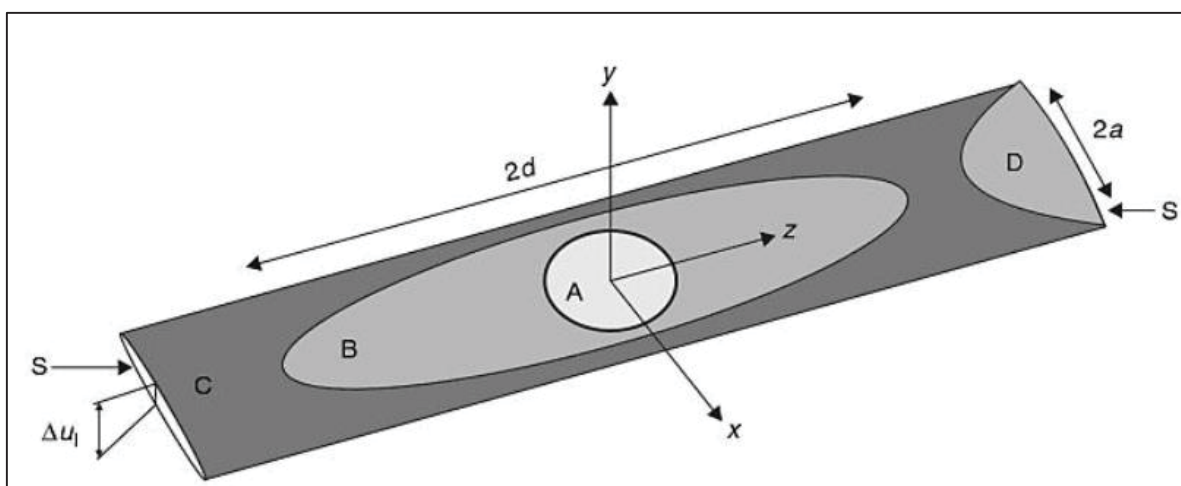
Figure 2. Ideal fracture geometries
A: Penny-shaped fracture, B: elliptical fracture, C: tunnel-fracture
(Gudmundsson, 2011)

Figure 2 shows ideal fracture geometries, A illustrates a penny-shaped interior fracture, B an elliptical interior fracture and C a tunnel shaped fracture. For elliptical fractures it is assumed that one dimension is commonly much larger than the other and the maximal displacement u_{max} occurs in its centre (Gudmundsson, 2011). An elliptic crack model is then calculated with help of its geometry. It results that the aperture which

has its maximum in the centre of the fracture is the normal opening displacement (u) multiplied with two.

As calculated fracture data also need to be compared with the measured one, FMI aperture data need to be considered. If no data are available to use the above described methods, Marret's (1996) proposed power law relationship needs to be taken into account. Bonnet et al. (2001) summarized studies of aperture distribution and showed the proposed exponets for aperture length power law relationship from various researchers (e.g. Barton and Zoback (1992), Johnston and McCaffrey (1996) and Barton (1995b)).

3.2 Stochastic fracture generation algorithms

The discrete fracture network models are generated with help of fracture statistics using FracMan by Golder Associates Inc. (2013) and StatFrac, a Rhino 5.0 Beta Plug-in, written by L. Mosser a student of University of Leoben, Austria. Object based stochastical modelling distributes points, here fracture centres according to a probability law, to this process random processes defining fracture size, fracture orientation, fracture spacing and P32 are attached. In Fracman truncation arises as an issue distorting the input fracture size distribution, because all parts of the fractures which are not within the model box are clipped without creating new fractures inside the box to reach the correct P32.

The conceptual models available for fracture network generation are the Enhanced Baecher Model, the Levy Lee Model and the Nearest Neighbour model. The algorithms to spatially place the fractures in StatFrac, are a Poisson Process or a Random Walk, which uses the Levy Lee process.

a. Enhanced Baecher model (EBM)

The Enhanced Baecher Model is an extension from the three dimensional Baecher Disk Model. The fundamental assumptions of Baecher Disk model (BDM) are that fractures are circular two-dimensional disks and the centre points of the fractures are randomly and independently spatially distributed forming a Poisson field. In general, the Poisson process comprised of the generation of random sets of discrete objects which may be point, lines or geometric figures such as polygons. Here this means that fractures are randomly spatially placed until a certain P32 is reached. The differences from BDM to EBM are, that the Enhanced Baecher Model allows fracture terminations at intersections with pre-existing fractures and that fractures are not true ellipses but polygonal approximations of ellipses. Fracture sets with relatively uniform distribution with minimal clustering are generated. The general input data needed are the fracture orientation (trend, plunge), a fracture size distribution and P32. Here additional data on fracture ellipticity/elongation and on termination probabilities for secondary fracture sets is required. The fracture spacing distribution is assumed to be normal distributed.

b. Levy Lee fractal model (LLFM)

A Levy Flight fractal process is used to produce smaller fractures around widely scattered larger fractures. This means a new center is created at a step from the previous one. A probability function is used to determine the length (L) of each step.

$$P(L'>L)=L^{-D} \tag{1}$$

Its direction is uniformly randomly distributed on the sphere. The size of the new fracture generated is proportional to the length of the step. The fractal dimension D used in the probability function for length determination dictates the geometry of the fracture system. Tighter clusters are produced with a high value of D and looser and more widely scattered clusters are generated with a lower value of D. Input data

required are fracture orientation (trend, plunge), a fracture size distribution, P32, fracture shape and the fractal dimension D.

c. Poisson Process in StatFrac

As already mentioned fractures are randomly spatially placed until a certain P32 is reached while using the Poisson Process. In comparison to the Enhanced Baecher algorithm StatFrac is able to account for the presence of a zone of relieved stress around fractures, the so-called "forbidden zone", where no other fracture of the same set could develop. According to Pollard (1990) there should be no other fracture of the same set inside this zone of relieved stress. Therefore if the "forbidden zone" of a bigger fracture intersects the zone of another smaller one, the fracture is removed. This process of checking for intersections and placing new fractures is continued until the desired P32 value is reached. The user input using the Poisson Process in StatFrac requires the fracture orientation (strike, dip), P32, fracture shape (elliptic, circular) and the forbidden zone geometry. Zones of relieved stress, forbidden zones, can be represented as spherical, cylindrical, or ellipsoidal volumes where the ellipsoid is the most realistic as this corresponds to the actual ellipsoid of stress around the fracture. The size of the zones scale with fracture half-length and multipliers are used to control the height and radius of the zones. The fracture spacing distribution is assumed to be normal distributed while using a poisson process.

d. Random Walk in StatFrac

The random walk based on the Levy Lee fractal process is used in StatFrac, with the difference that it is expanded with a check for "forbidden zones". This means the centres generated with a certain step from the previous one are followed by a "forbidden zone" check. The same input as for the poisson process used in StatFrac is required, with the difference that the spacing distribution is predefined as a user input.

Table 1 summarizes the underlying assumptions made using the different stochastic fracture generation algorithms. The fracture orientation is set constant for every set to be able to analyse the impact of the different orientations on kequ. and qf/qm.

Enhanced Baecher Model (FracMan)	Poisson Process (StatFrac)	Random Walk (StatFrac)
• Fracture shape: circular • Fracture length distribution: power law • Fracture set orientation constant for every set • Fracture intensity constant (0.07 m²/m³)		
• Fracture shape: polygonal approximations of circles		• Center points are set according to a probability function of the length from the previous to the next center point
• Fracture Spacing: normal distribution • Center-points of fracs are randomly and independently distributed in space forming a poisson field		• Fracture spacing: power law distribution (user input)
	• Account for forbidden zones: cylindrical shape of zone of relieved stress	

Table 1. Underlying assumptions for the stochastic fracture generation methods

3.3 Meshing with ANSYS

Discrete fracture geometries need to be subdivided into smaller and simpler elements as these geometries are a necessary input in the simulation process. In this study Finite Element method (FEM) is used to discretize the governing equations, there the generated mesh has a direct influence on the accuracy of the results. A too coarse mesh would not cover the full complexity of a NFR and a too fine would lead to high computational expenses. An unstructured grid is used as it captures the full complexity of the DFM model. To generate this volume mesh out of the DFM models, the ANSYS meshing tool is used. To get a more homogeneous result and to increase mesh quality, the mesh can be made very fine with the "smoothing" option and then coarsened again to reduce the amount of elements and nodes for the computation afterwards. Before the input files for the simulator can be exported it is necessary to check the mesh on

problems, like e.g. stand-alone surface mesh or non-manifold vertices, as poor quality elements influence the computational result in a bad way. In case of a not positive response of the mesh check, the mesh needs to be improved with the repair option on ANSYS to assess mesh quality.

3.4 Flow based upscaling

In this section the governing equations used are explained. Darcy's law is inserted into conservation of volume equation to find pressure equation.

$$\nabla u = 0 \tag{2}$$

$$\nabla \frac{k}{\mu} \nabla p = 0 \tag{3}$$

u – Darcy velocity
p – fluid pressure (Pa)
μ - dynamic viscosity (Pa s)
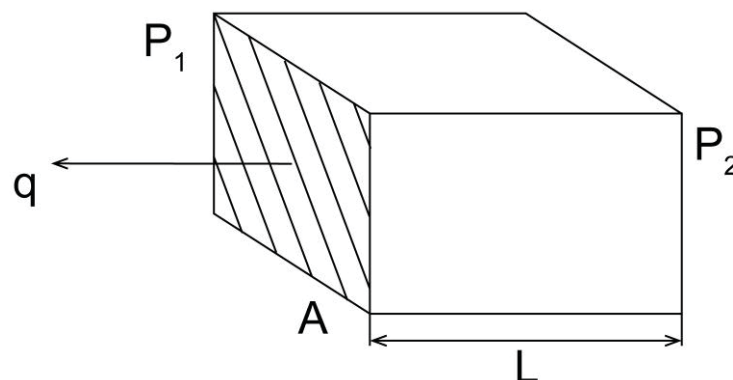
Figure 3. Definition and direction of governing equation

Fractures and matrix are discretized using Finite Element Method (FEM) with piecewise constant properties. As boundary condition it is assumed to have a fixed p inlet and a fixed p outlet on two opposing sides, all other boundaries are assumed to be no flow boundaries. For matrix elements, permeability k is considered to be matrix permeability and for fractures, fracture permeability is calculated using the parallel plate law. The assumption using general parallel plate law is to have laminar flow and a fracture with a smooth, parallel surface and that the length of the plates is more than

three times than the distance between them (l>> b). Snow (1969) proposed the equation for a velocity profile between two plates as following:
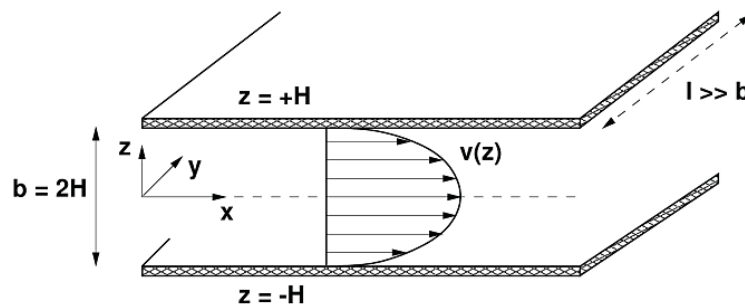
Figure 4. Laminar flow between two parallel plates

Figure 4 shows the parabolic velocity profile as a result from laminar flow between two plates. (Dietrich, et al., 2005) Having this parabola-shaped profile, the integral results in:

$$v_x = \frac{1}{2\mu}\frac{dp}{dx}(y^2 - hy) \tag{4}$$

$$q = \int_0^H v_x dy = -\frac{1}{12}\frac{h^3}{\mu}\frac{dp}{dx} \tag{5}$$

Comparing formula 5 to Darcy's law shows that permeability derived from parallel plate law concept is proportional to the square of fracture aperture b:

$$k = \frac{b^2}{12} \tag{6}$$

Generally, the fluid velocity follows the first term of the cubic law as it is proportional to the cube of aperture:

$$q \propto \frac{b^3}{12\mu}\nabla p \tag{7}$$

3.5 $k_{equ.}$ + q_f/q_m calculation for the field scale model

Formula 8 introduces the general concept of equivalent permeability calculation (Matthäi & Nick, 2009).

$$k_{equ} = \frac{q\mu_w L}{A(p_{outlet} - p_{inlet})}$$
(8)

A - Area (m²) of model cross section perpendicular of the flow
L – Length (m) of model in direction of flow
P_{inlet}, p_{outlet} – Inlet and outlet fluid pressure (Pa)
q – Total flux through model

Respective to equivalent permeability calculation the fracture/matrix flux ratio can be calculated. This ratio shows how much the flow of the rock matrix influences the total flow. So a small value would mean that the rock matrix dominates the flow. The higher the value gets the lower the contribution of the rock matrix.

$$\frac{q_f}{q_m} = \frac{q_{total}}{\nabla p \frac{k_m}{\mu}}$$
(9)

3.6 Sensitivities and experimental design of the models

In general a model is an imperfect copy of reality and is exposed to some sensitivity. For the experimental design it is necessary to have a look on the sensitivities of the stochastic fracture models. The first sensitivity is the use of different stochastic fracture generation algorithms, as every algorithm has its own assumptions. This stochastic fracture generation leads me to an additional sensitivity, as for same input properties different fracture geometries were generated. The stochastic generation of the fracture networks influences the number of fractures, fracture intensity and the fracture length distribution in the model. Also the model size influences the accuracy of the results and therefore is a sensitivity parameter. The model must be bigger than the mode of the fracture size to get an acceptable uncertainty. The DFM model is also sensitive to a variation of rock matrix permeability. Also in flow based upscaling a sensitivity occurs

as it highly depends on boundary conditions and is influenced by them. The big question here is how to deal with these sensitivities and how many models are enough to cover the full range of possible results in the stochastic generation process. In Table 2 the experimental design is presented.

Characterisation of the NFR
Build DFM model from fracture statistics obtained from borehole data
Stochastic generation of equi-probable DFM realisations
Stochastic fracture generation algorithms: • Enhanced Baecher Model (FracMan) • Poissson Process (StatFrac) • Random Walk (StatFrac)
Variation of model size (side length): 25, 50, 100 meter
50 equi-probable realisations per model size
Analysis of geostatistical properties of DFM models
Set by set confirmation
Cluster analysis
Meshing with ANSYS
Flow based upscaling to obtain properties of fracture-matrix ensemble:
$K_{equ.}$ – qf/qm tool by CSMP++
Steady state single-phase fluid flow
Variation of matrix permeability (5 mD, 5 mD, 50 mD)
Using configuration file for fracture permeability (a²/12 for each fracture)
BCs: fixed p inlet & outlet for two opposing boundaries, no flow for all others
OUTPUT: $k_{equ.}$ and qf/qm

Table 2. Overview: From NFR field data to $k_{equ.}$ and qf/qm

4. Application to Tensleep Formation (Sandstone B)

In this part of my thesis I will analyse the statistical data from Teapot Dome dataset to get the input necessary for the stochastic model generation. Also the realisation of the models will be shown.

4.1 Statistical analysis of Tensleep fracture data

To generate a discrete fracture and matrix model, the matrix and especially the fracture sets need to be characterized as accurately as possible. NFRs are highly heterogeneous and complex, so the characterization is much more difficult and even more important to get precise results. I start with the fracture set characterisation, which is coupled with fracture orientation, as fractures with the same orientation form a fracture set. With help of FMI orientation data a rose diagram has been generated using the software TectonicsFP to identify the different fracture sets. As I just had the dataset of well 48-x-28, fracture strikes of this well are shown in Figure 5. Terzaghi approach was used to correct the fracture orientations. Four dominant fracture sets coexist in Tensleep formation. This fracture sets are interpreted to have formed through deformation associated with the Laramide (late Cretaceous to early Tertiary) (Cooper, 2000).
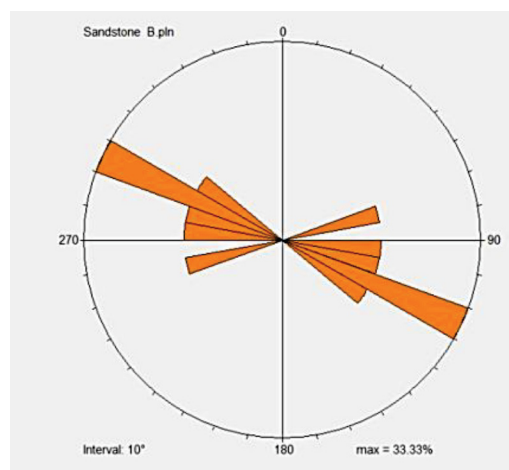

Figure 5. Well 48-x-28 Rose diagram Sandstone B fracture strikes

Table 3 summarizes the fracture orientation data for the four existing fracture sets.

	Fracture Set	Mean Strike	Mean Dip
B Sandstone	1	88	358
	2	110	20
	3	153	63
	4	130	40

Table 3: Fracture orientation data

- Fracture set orientation data generated with help of the rose diagrams was used. As data for well 48-x-28 have not been enough, data from Smith (2008) have been used to cross check the generated results and to complete them.

At least 200 individual measurements would be necessary to fit a distribution curve to fracture spacing and length data (Priest & Hudson, 1976). As just data for one well (48-x-28) have been available, literature data have been looked up, as many researches with an acceptable amount of data have already been made. Gilbertson (2002) observed a power law distribution for spacing in Tensleep formation. Wilson, et al. (2013) showed that the spacing distribution follows a power law over a limited scale of range. The power increases with an increase in spacing. The FMI data provided for well 48-x-28 showed a mean spacing of 5.5 meters for the spacing, so also the spacing distribution for this range of spacings was used, which leads to a power of -0.47. Calculating fracture density P10 and then fracture intesity P32 with this mean spacing would lead to an overestimation of P32 (0.18 m²/m³). Fracture intensity in previous works proposed a P32 between 0.02 and 0.075 m²/m³. In this thesis a P32 of 0.07 m²/m³ was used.

Many researchers (e.g.: (Cooper, 2000) (Cooper & Lorenz, 2001) (Schwartz, 2006) (Smith, 2012) (Wilson, et al., 2013)) proposed the fracture length to be power law

distributed. Fracture lengths in Tensleep formation range from 0.47 to 27.42 meters (Schwartz, 2006). The lower-off necessary for power law distribution is 0.5 meter and the upper is 27.4 meters, so the whole range of fracture length is used.

A power law relationship between aperture and length was used to estimate fracture length in the Tensleep. As no of the exponents for power law aperture length relationship proposed is valid for fracture length between 0.5 and 27.4 meters and apertures between $1.73*10^{-4}$ and $2.28*10^{-6}$, a different way to get a relationship has to be found. It is not possible to simply change the constant and/or the exponent to fit a power law aperture length relationship. Schwartz (2006) proposed to use Oskaya's (2003) minimum fracture length method. The minimum fracture length was approximated from average FMI aperture data. This method leaded to a constant of 0.000041, for the exponent Perez (2002) value was used (0.884). Perez (2002) proposed relationship: aperture (mm) = $0.012*length$ (mm)$^{0.884}$, which is valid for micro-fractures

In the flow upscaling process also the rock matrix properties of Tensleep formation are needed. Results of Core analysis of well 48-x-28 indicates the eolian sandstone to be fine to very fine grained, well sorted and quartz cemented. Figure 6 shows the porosity-permeability plot for the Tensleep Formation (Sandstone B), a high variation is clearly visible. For the simulations different matrix permeability scenarios (5, 50, 500 mD) were calculated, matrix porosity is not required as an input for the $k_{equ.}$ calculator.
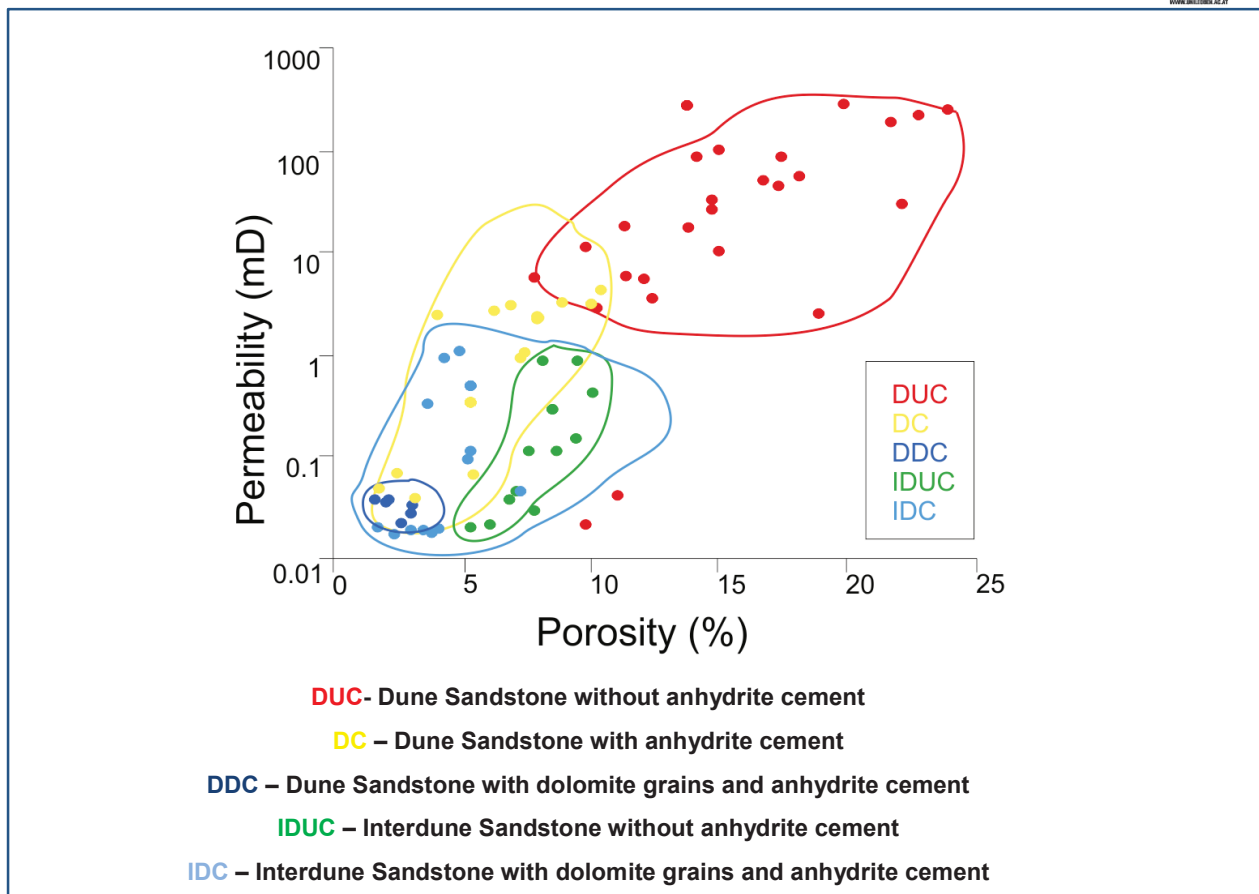
Figure 6. Poro-Perm Plot for Tensleep Formation (Yin, 2005)

4.2 Model Setup

The model consists of one simplified layer of Sandstone B. A model domain of 25*25*25, 50*50*50 and 100*100*100 cubic meter was used and meshed with triangular elements (about 14,000,000 elements). A rock matrix permeability of 5 mD was used. To see the influence of rock matrix, the permeability was then increased to 50 mD and 500 mD. Fracture permeability was calculated for every single fracture using parallel-plate law. In sum the fracture sets (all 4 sets) consist between 1100 and 1700 fractures. The flow equations have been discretized using first order Finite Element formulation. Fixed inlet and outlet pressures are assumed as boundary conditions for two opposing boundaries. All the other sides are no flow boundaries. A horizontal directional stress was assumed.

4.3 Model Realisations

The summary of the necessary input for the stochastic fracture set generation is shown in Table 4. Fracture orientation is held constant as I wanted to see the orientation effect of every single set. Model realisations for all used stochastic generation methods are shown in Figure 7. Each, the realisation with the lowest and the highest number of fractures is shown.

	FracMan	StatFracGUI	StatFracGUI
Generation model	Enhanced Baecher	Poisson Process	Random Walk (Levy Process)
P32	0.07		
Fracture orientation ➔ constant	trend/plunge	strike/dip angle	
Fracture size distribution	Pareto power Law	power function	
Spacing distribution	normal (predefined)	normal (predefined)	power-law (user input)
Forbidden zone geometry	-	cylinder (height & length multiplier)	

Table 4. Summary of fracture set generation input

In Figure 7 each 2 examples of stochastically generated DFM models are shown. Using a Poisson process for stochastic fracture set generation, the spatial placement of the fractures looks homogeneous. This means the fractures are equally distributed over the whole volume of the model and no part of the volume is without fractures. Using Poisson process in FracMan the models are in 90 % of the combinations equally distributed so as in StatFrac. Still a quality check has to be made, as some model realisations especially using a Random Walk are very heterogeneous and in some parts of the model no fractures are placed, as the algorithm has reached P32 before fractures could have been placed in this region.

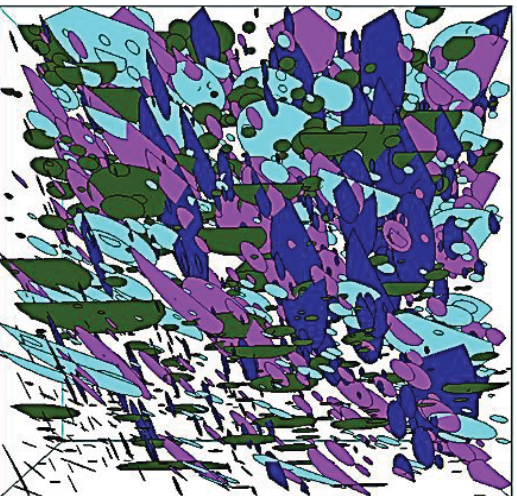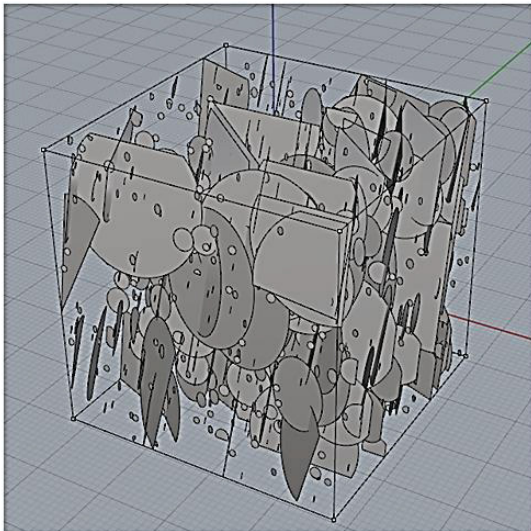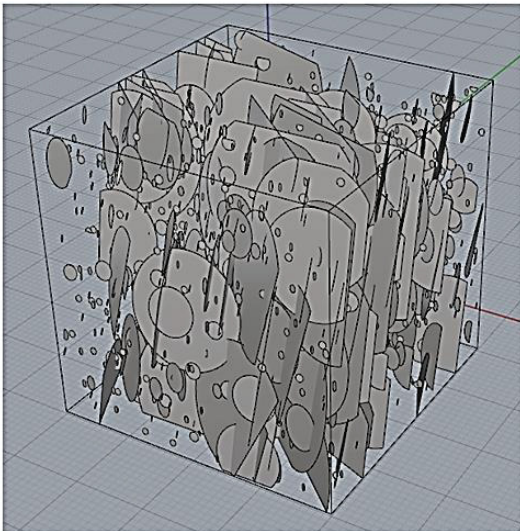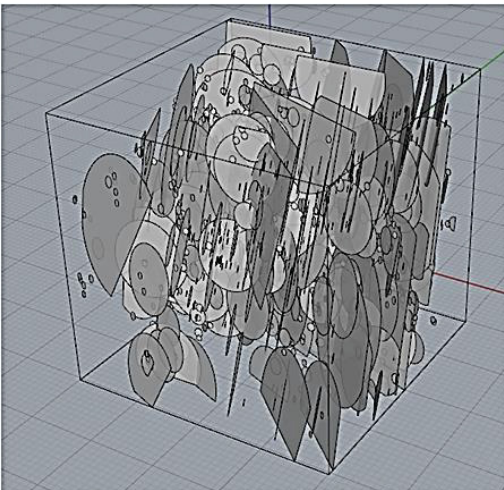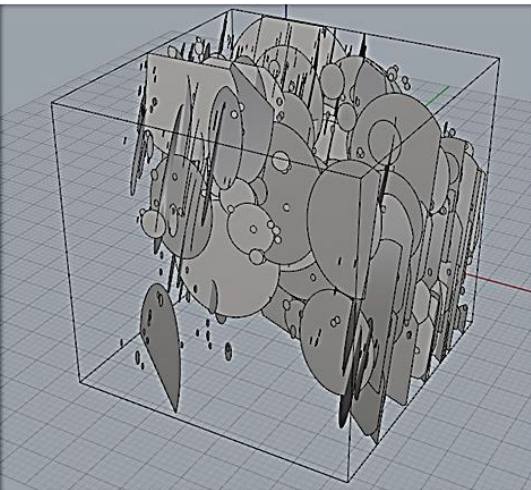|	n=1357	n=1685
Enhanced Baecher FracMan		
	n=1175	n=1546
Poisson Process StatFrac		
	n=1185	n=1470
Random Walk StatFrac		

Figure 7. Examples of realisations for each stochastic fracture generation method

5. Results

In this part of my thesis the results of the geometrical analysis of the fifty stochastically generated DFM realisations (Sandstone B – fracture set 1) for different fracture generation algorithms and model sizes are shown. Following the results of a cluster analysis are presented. For DFM representations in StatFrac a separate script to locate and count the fractures has been written (Appendix A). Finally, I show the results of the flow data analysis.

5.1 Geometric analysis of the stochastic DFM realisations

The stochastic generation of the fracture realisations has the effect that for the same input different fracture geometries arise. This has an effect on the number of fractures generated in the model, fracture intensity and the fracture length distribution.

- **Fracture intensity – P32**

First the input fracture intensity will be compared with the one achieved for the different fracture set realisations. The input value for P32 was 0.07 m²/m³. In Figure 8 a Pareto chart is shown to see the variation of the fracture intensity output of the fifty different realisations. Furthermore the minimum and maximum output values for P32 are summarized. Fracture intensity gets more accurate with increasing model size. In general more accurate results could be achieved using stochastic fracture generation algorithms of StatFrac. A bigger model size is needed while using fracture generation algorithms in FracMan to reach the wanted P32 with a low deviation from the input. For the biggest model size (model edge length of 100 [m]) the error is even lower than 1% for both stochastic fracture generation algorithms.
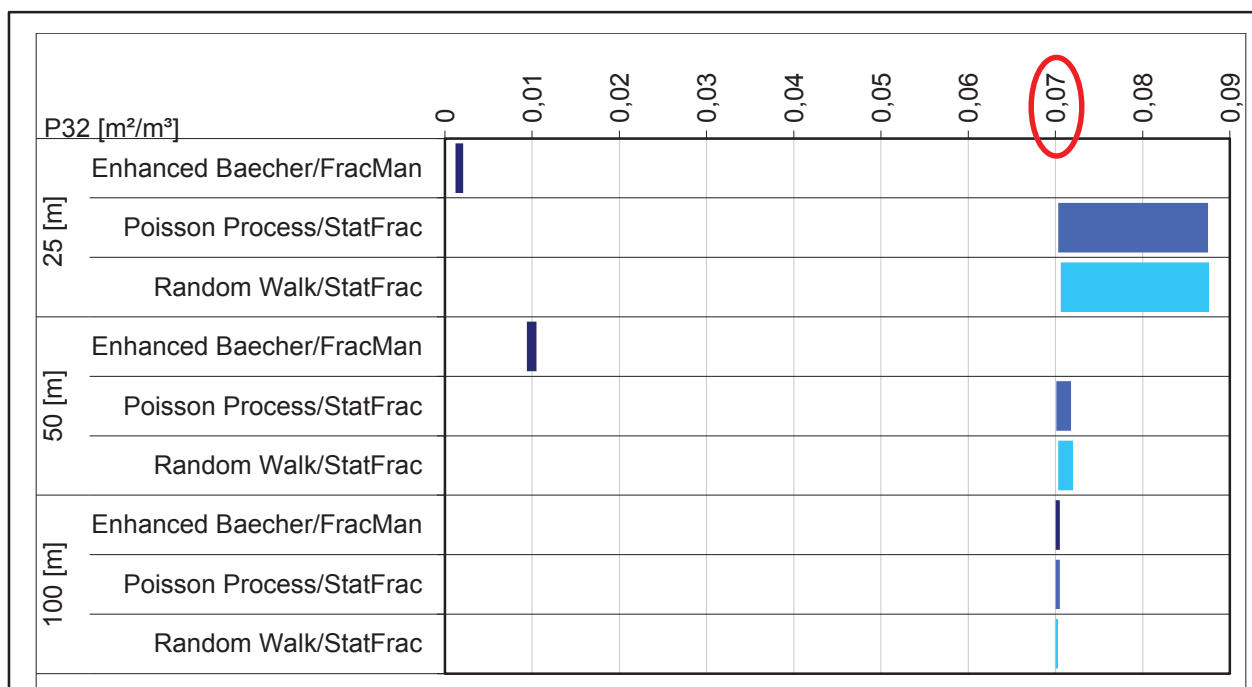
Model edge length	25 [m]	50 [m]	100 [m]
MIN			
Enhanced Baecher / Fracman	0.0012	0.0094	0.07003
Poisson / StatFrac	0.0703	0.0701	0.07001
RandomWalk / StatFrac	0.0706	0.0703	0.070006
MAX			
Enhanced Baecher / Fracman	0.0021	0.0105	0.0705
Poisson / StatFrac	0.0875	0.0718	0.0705
RandomWalk / StatFrac	0.0876	0.0720	0.0703

Figure 8. Fracture intensity P32 as a function of box volume

- **Number of fractures**

The number of fractures grows with increasing model size and varies among the algorithms that place the fractures. The Enhanced Baecher model used in FracMan in general generates a higher number of fractures within a fracture set. Furthermore a higher variation of the number of fractures is achieved, compared to the Poisson process and the random walk in StatFrac.

Number of fractures [-]			

Model edge length	25 [m]	50 [m]	100 [m]
MIN			
Enhanced Baecher / Fracman	22	286	2751
Poisson / StatFrac	32	263	2482
RandomWalk / StatFrac	40	244	2797
MAX			
Enhanced Baecher / Fracman	113	575	3409
Poisson / StatFrac	80	432	2909
RandomWalk / StatFrac	95	385	3067
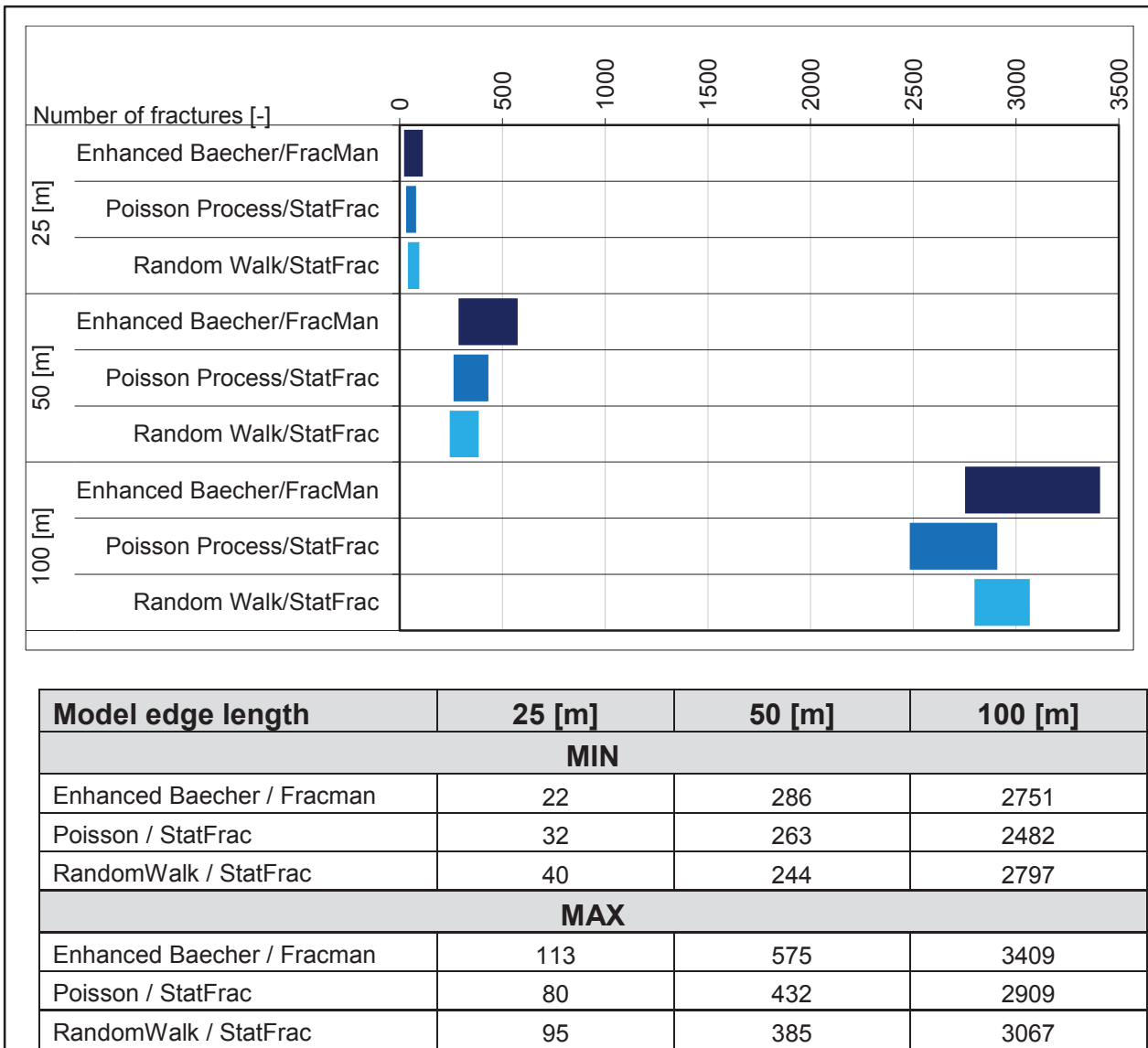
Figure 9. Number of fractures as a function of box volume

With increasing model size also the array of number of fractures increases. While the difference between the minimum and maximum number of fractures using e.g. Enhanced Baecher model for the smallest model size is 91, it increases exponentially to 658 for the biggest model size. This increase of number of fractures per equi-probable set also leads to a higher uncertainty in the different results, as the difference also influences the number of clusters and so, the flow through the fracture network. Figure 10 shows the number of fractures with an increasing model box side length in a log-plot. The number of fractures increases linearly.

Figure 10. Number of fractures

Figure 11. Frequency plot for number of fractures

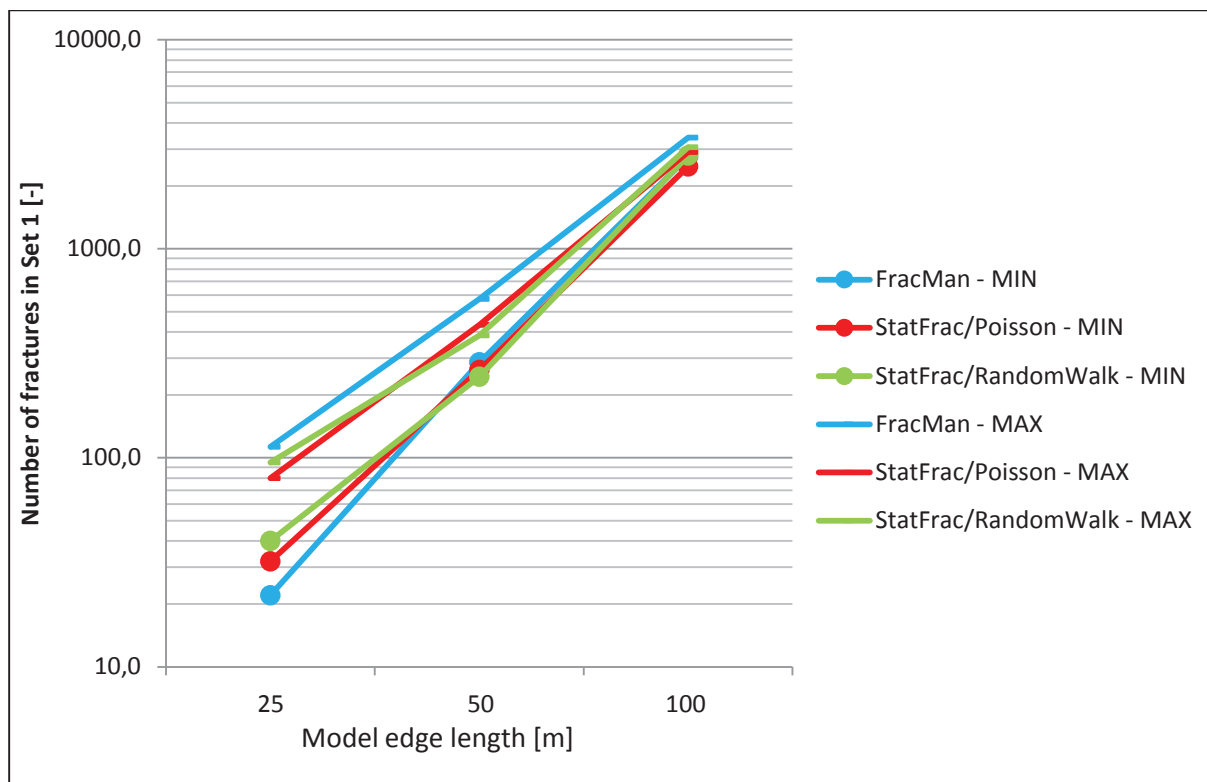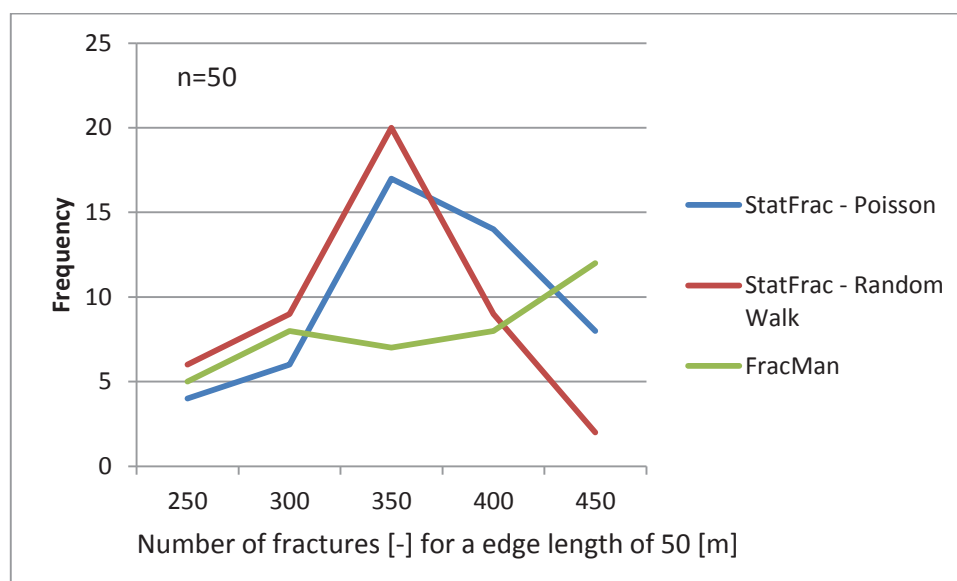Figure 11 displays a frequency plot for the number of fractures generated. The number of fractures generated in StatFrac in a box with a size length of 50 m is normal distributed, while in FracMan no real trend can be obtained. It seems that, also if the

software uses the same stochastic fracture generation algorithm, here a poisson process, different results are achieved, which might be caused by the forbidden zones.

- **Max. fracture radius**

As big fractures have a high influence on fracture connectivity and are therefore key for fracture percolation, I looked for the maximum fracture size in every realisation. Since there is no REV, the maximum fracture radii increase with increasing model size. Before I go into detail with the maximum fracture radii, I will show the power law fracture size distribution for the realizations with the minimum and the maximum number of fractures.

Figure 14, Figure 13 and Figure 14 show the frequency distribution for fracture radii. The blue line on the figures represents the associated cumulative distribution, which gives the probability of a fracture radius to have this size or larger for a certain fracture radii. The bigger the model gets, the higher the probability to get big fracture radii. In all models P90 is between 4.9 and 5.1 meters. So there is little variation of the probability for fractures with a radius this size or larger.

I plotted the fracture set with the highest and the lowest number of fractures for every software tool, to see if also the number of fractures between 5 and 13.7 meters changes. For the Poisson process and the random walk used in StatFrac there are just small differences, but the Enhanced Baecher model used in FracMan shows higher differences, as there have been generated 10 fractures less in the set with the lowest number than in the one with the biggest number. This lack of "big" fractures in the model with the lowest number of fractures could have a not negligible effect on percolation.

Figure 12. Frequency distribution and CDF – 50³ [m³] – Poisson process/StatFrac
    a.) Fracture realisation with the lowest number of fractures generated
    b.) Fracture realisation with the highest number of fractures generated

Figure 13. Frequency distribution and CDF – 50³ [m³] – Random Walk/StatFrac
a.) Fracture realisation with the lowest number of fractures generated
b.) Fracture realisation with the highest number of fractures generated

The Enhanced Baecher Model in FracMan generates between 6 and 8 times less fractures with a radius between 0.56 and 1 meter, compared to StatFrac fracture sets. Most fractures are in a range between 1 and 2 meters and then the frequency distribution shows the same decrease which reveals to power law like the ones generated in StatFrac. Using the Enhanced Baecher model in FracMan fracture sets were generated according to the data input, in a second step the created fractures need to be truncated / clipped that no part of a fracture is outside the model box. This

process of clipping may destroy the input statistics, as the fracture length distribution changes from power law to a lognormal distribution. Fracture length statistics varies as the centres of fractures are not all inside the box, so fracture radii might change to smaller ones during the clipping process, which leads to an increase in medium fracture radii.
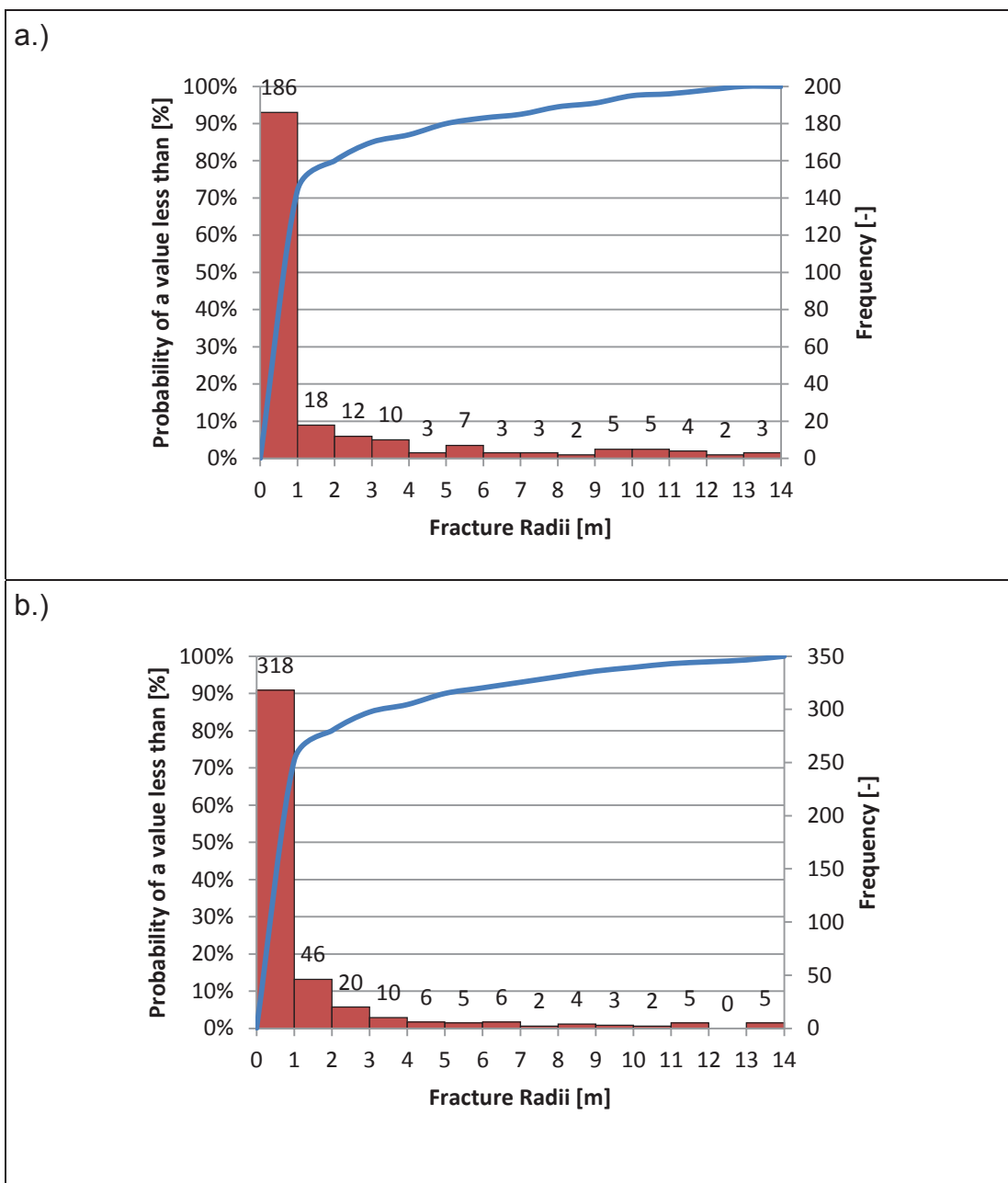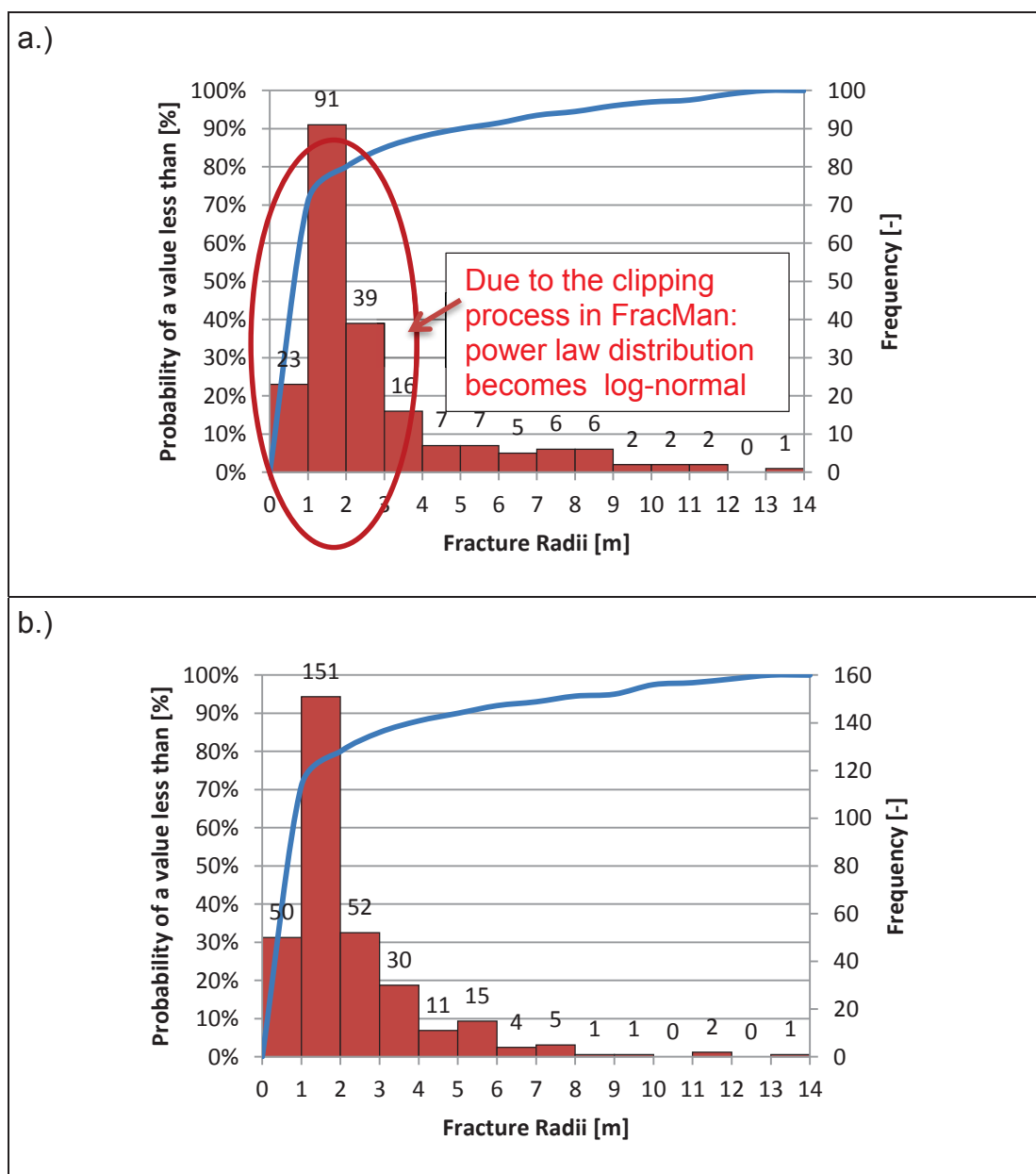

Figure 14. Frequency distribution and CDF – 50³ [m³] – Enhanced Baecher model
a.) Fracture realisation with the lowest number of fractures generated
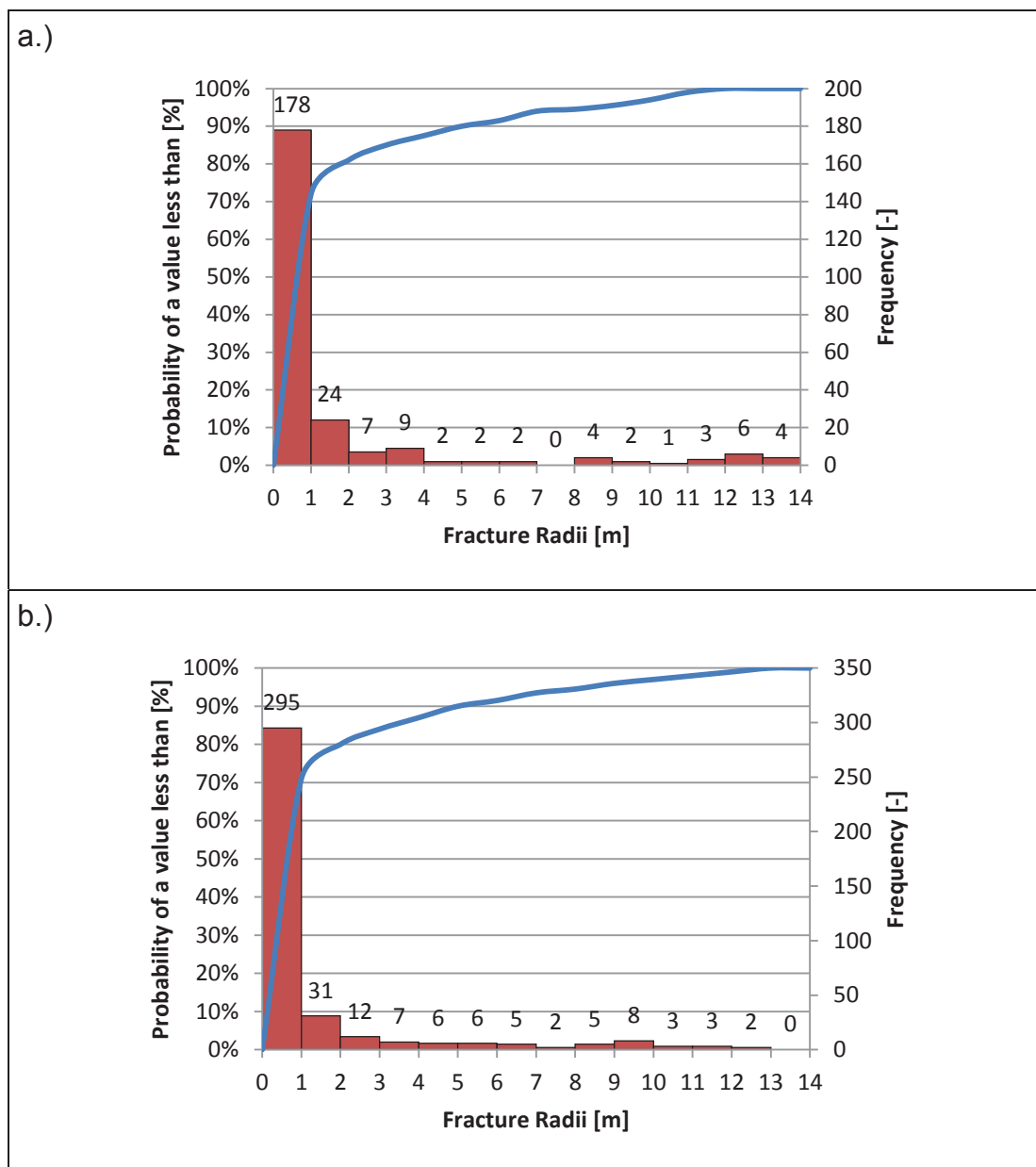b.) Fracture realisation with the highest number of fractures generated

In Figure 15 the variation of the actual maximum fracture radius to the input (13.7 [m]) is shown.
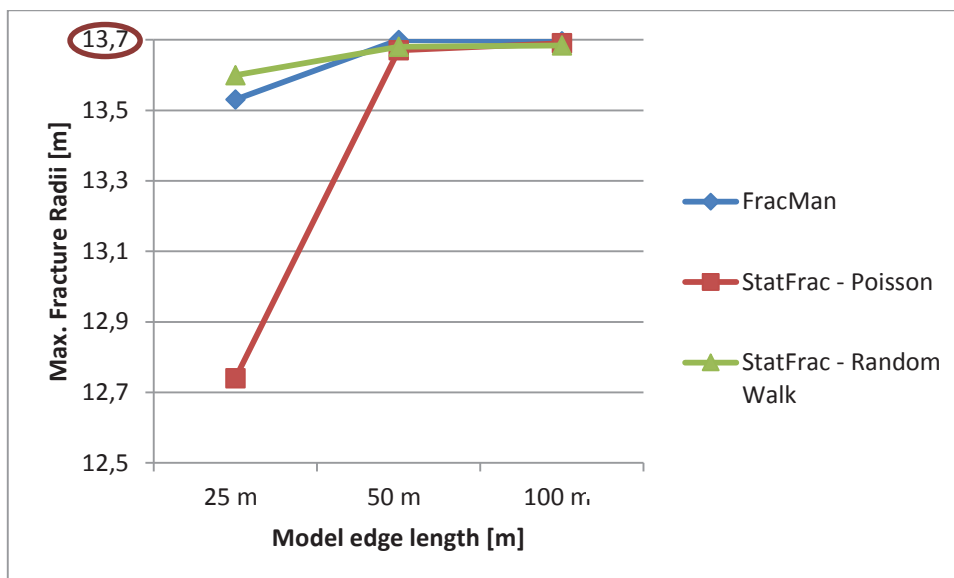
Figure 15. Maximum fracture radius (Mean of 50 realisations)

The range of maximum fracture radius, which represents the half-lengths of fractures, decreases with increasing model size. For the smallest model edge length (25 m) the maximum fracture radius is arranged between 12.7 and 13.6 meters, for the medium model edge length (50 m) the range decreases and lies between 13.67 and 13.699 meters. For the biggest model edge length (100 m) the maximum error is 0.12 %. Concluding, an increase in model size leads to a result closer to the input maximum fracture radius (13.7 meter) and this has in turn a positive effect on flow. Results also show that the Random Walk used StatFrac and the Enhanced Baecher model used in FracMan lead to more accurate result than the Poisson algorithm. In most models about 5 fractures with a radius between 13 and 13.7 meters are found.
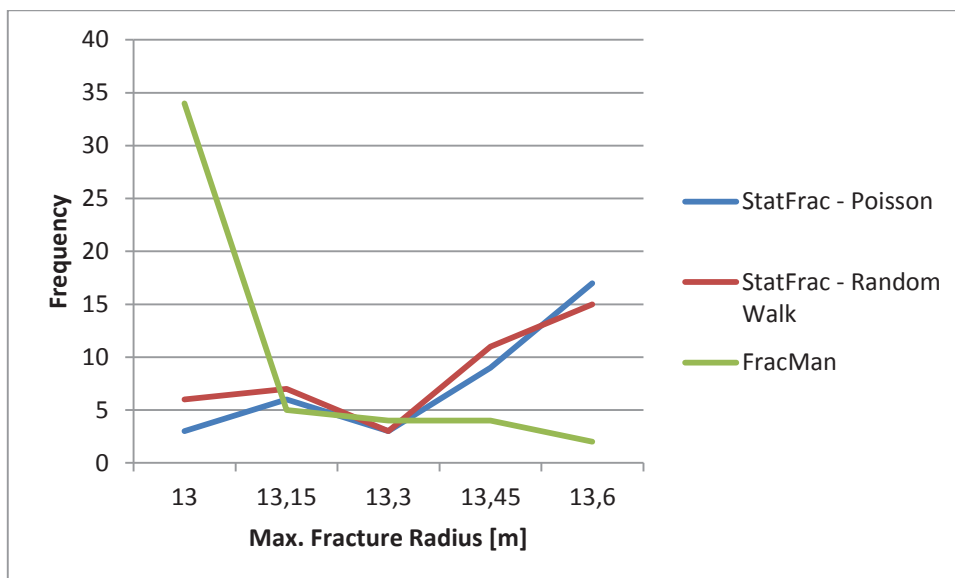
Figure 16. Frequency plot for maximum fracture radius

Figure 16shows that in FracMan the maximum fracture radius fits to an exponential decay, which leads to a higher error in most of the equi-probable models as the maximum fracture radius is defined to be 13.7 meters. StatFrac – Poisson - delivers a quite similar frequency distribution as StatFrac – Random Walk - with a trend to have more equi probable models with values near the defined radius.

Table 5 summarizes the uncertainty between input and output of P32 and maximum fracture radius, including the estimated uncertainty in percent.

Model edge length [m]			25	50	100
			Uncertainty		
Enhanced Baecher / FracMan	$P32\ [m^2/m^3]$	Input: 0.07	+ 0.000 - 0.0679 (97%)	+ 0.0000 - 0.0595 (85%)	+ 0.0005 (0.7%) - 0.0000
Poisson Process / StatFrac			+ 0.0175 (25%) - 0.0000	+ 0.0018 (2.6%) - 0.0000	+ 0.0005 (0.7%) - 0.0000
Random Walk / StatFrac			+ 0.0176 (25.1%) - 0.0000	+ 0.0020 (2.9%) - 0.0000	+ 0.0003 (0.4%) - 0.0000

Model edge length [m]			25	50	100
Enhanced Baecher / FracMan	Max. fracture radius [m]	Input: 13.7	+ 0.00 - 0.17 (1.2%)	+ 0.00 - 0.03 (0.2%)	+ 0.00 - 0.01 (0.07%)
Poisson Process / StatFrac			+ 0.00 -0.96 (7%)	+ 0.00 - 0.02 (0.15%)	+ 0.00 - 0.001 (0.01%)
Random Walk / StatFrac			+ 0.00 - 0.10 (0.7%)	+ 0.00 - 0.001 (0.01%)	+ 0.00 - 0.001 (0.01%)

Table 5. Results of uncertainty analysis

The highest uncertainty for P32 occurs in FracMan. While the obtained uncertainty in percent is about 3% for StatFrac fracture generation algorithms, the Enhanced Baecher Model in Fracman still has an uncertainty of 85%. Errors for the maximum fracture radius are negligible with a model edge length of 50 meter and 100 meter, as they are below 1%.

Before creating equi-probable fracture set realizations for each set in Sandstone B to study different realization combinations of the sets, the appropriate model size has to be chosen. My aim while choosing the best model size was to have a low uncertainty for the different parameters e.g. P32, maximum fracture length and variation of number of fractures and still have an acceptable expenditure of time to generate the sets. I decided to create Sandstone B with its different equi-probable fracture sets with a model edge length of 50 m. Model edge length 50 m has been chosen because the uncertainty (below 5% for StatFrac fracture generation algorithms) with this model size is acceptable and a bigger model size leads to a longer computational time for generation of the sets and further also for the meshing and simulation process.

5.2 Cluster analysis

The most important thing in this study of equi-probable fracture set combinations is to see the impact of fracture arrangement on equivalent permeability, fracture matrix flux ratio and percolation. To distinct percolating and non-percolating clusters is very important as fluid flows only in the percolating connected fractures, while it doesn't flow in the non-percolating parts (Adler & Thovert, 1999). A system percolates if the flow is able to go through the whole model, e.g. from the left model boundary to the right model boundary.

The more fractures are in the system, the higher the probability that they are connected to each other forming clusters. Reliant on fracture orientation of the different sets, size distribution, fracture density and spatial distribution more or less cluster form within a model (Odling, et al., 1999). In general it is more likely that long fractures intersect each other or connect with other smaller fractures (Odling, et al., 1999).

For each fracture set 10 equi-probable realizations have been generated and then randomly combined in FracMan and in StatFrac, to see the variation of the different combinations concerning number of fractures in the model, clustering etc..

First I wanted to know how the total number of fractures is related to the ratio of clusters divided to the total number of fractures In Figure 17 it is visible that the ratio varies with the number of fractures in the combination. The highest variation is achieved using the Poisson process in StatFrac and the lowest using the Enhanced Baecher model in FracMan.
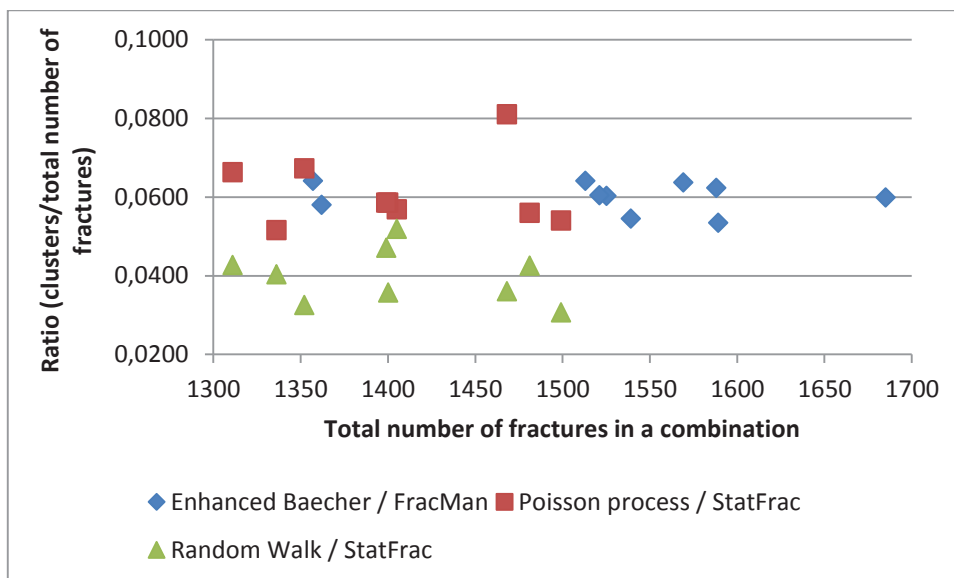
Figure 17. Ratio clusters/n-fractures related to the number of fractures

Figure 18 shows the variation of the total number of fractures which are interconnected in different clusters of the 10 equi-probable combinations. Just a narrow range between the different combinations can be obtained. Using the Enhanced Baecher model in FracMan 32% (mean) of the fractures form a cluster. In StatFrac the Random Walk and also the Poisson process deliver quite similar results with 27% and 31%. The low percentage can be ascribed to the power law distribution of the fracture length, as a high percentage of small fractures are distributed in space.

In general a big fracture has a higher possibility to have an intersection with other fractures. The more medium to big fractures are in the same region of the model, the higher is the chance that they intersect each other and also smaller fractures, which increases the number of fractures in a cluster.
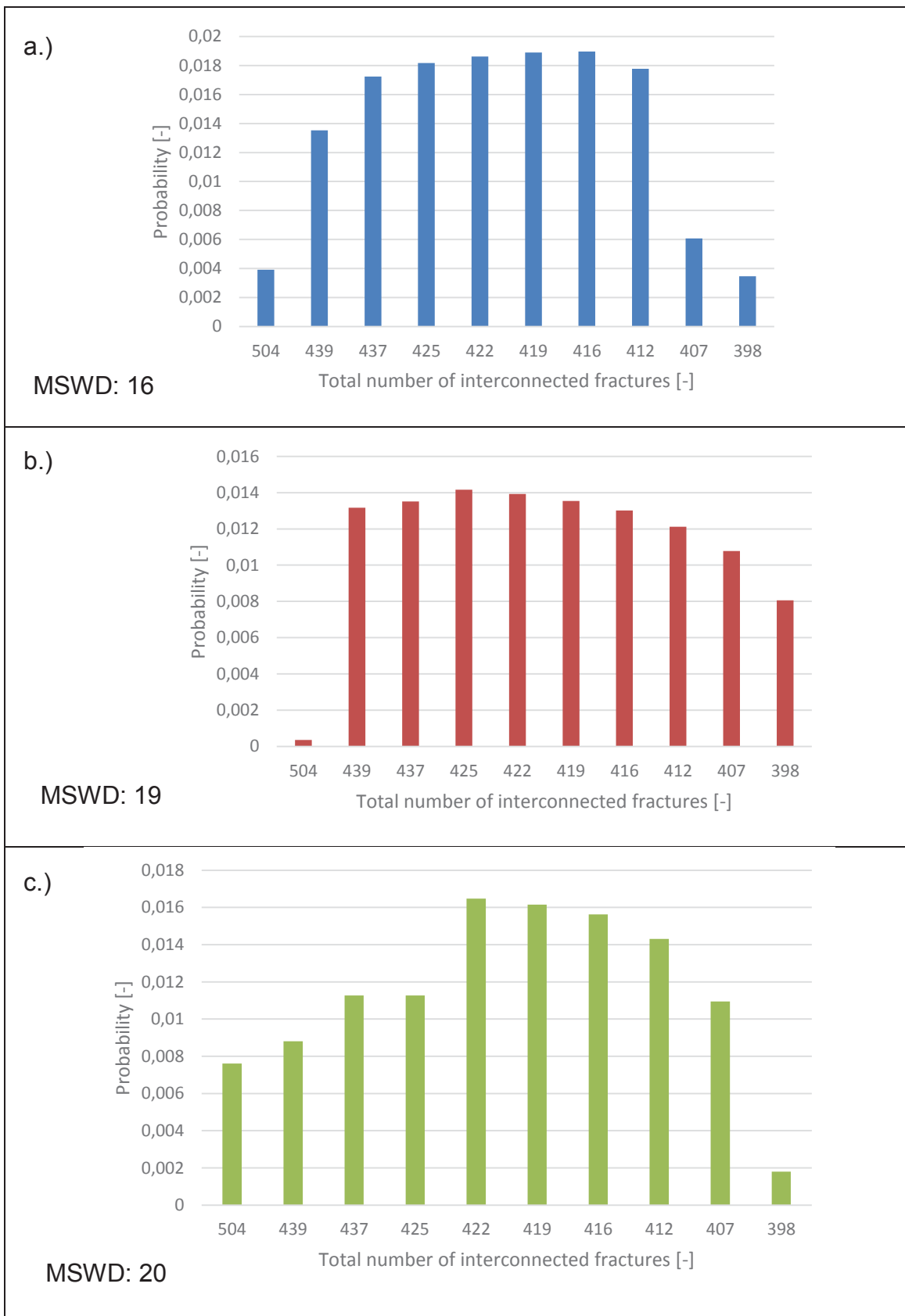
Figure 18. Total number of interconnected fractures
a.) Enhanced Baecher/FracMan; b.) Poisson Process/StatFrac; c.) Random Walk/StatFrac

Next I have a look on the variation of the size of the largest cluster in the different combinations. Figure 19 shows the average sizes of the largest cluster of the 10 combinations. The standard deviation was used to create the error bars.
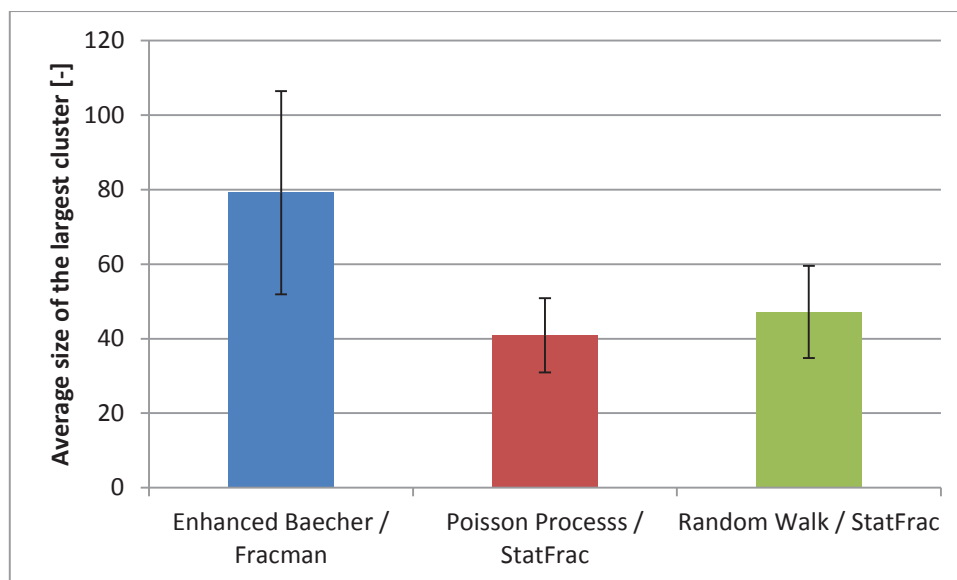
Figure 19. Average size of the largest cluster

Figure 20 shows the combined fracture area for the biggest cluster in each of the randomly chosen combinations.
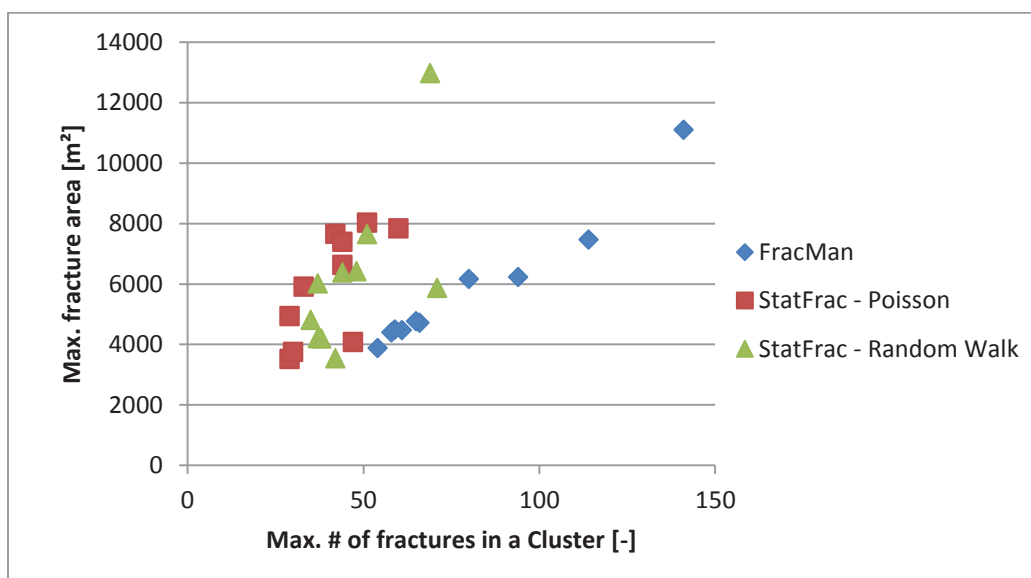
Figure 20. Max. fracture area vs. max. number of fractures in a cluster

Also here the results in the different combinations aberrate, which have a huge effect on flow pattern and leads me to the assumption that also quite diverse simulation

results will be obtained. The fracture area of the biggest percolating clusters comprises in between 11% to 32% of the total fracture area in FracMan, 9% to 21 % in StatFrac using the Poisson Process and 10% to 39% using the Random Walk. This again is a big range.

	Enhanced Baecher model / FracMan	Poisson process / StatFrac	Random Walk / StatFrac
Mean	1525	1387	1287
St.Dev.	95	98	81

	Enhanced Baecher model / FracMan	Poisson process / StatFrac	Random Walk / StatFrac
Mean	92	85	56
St.Dev.	7	12	9
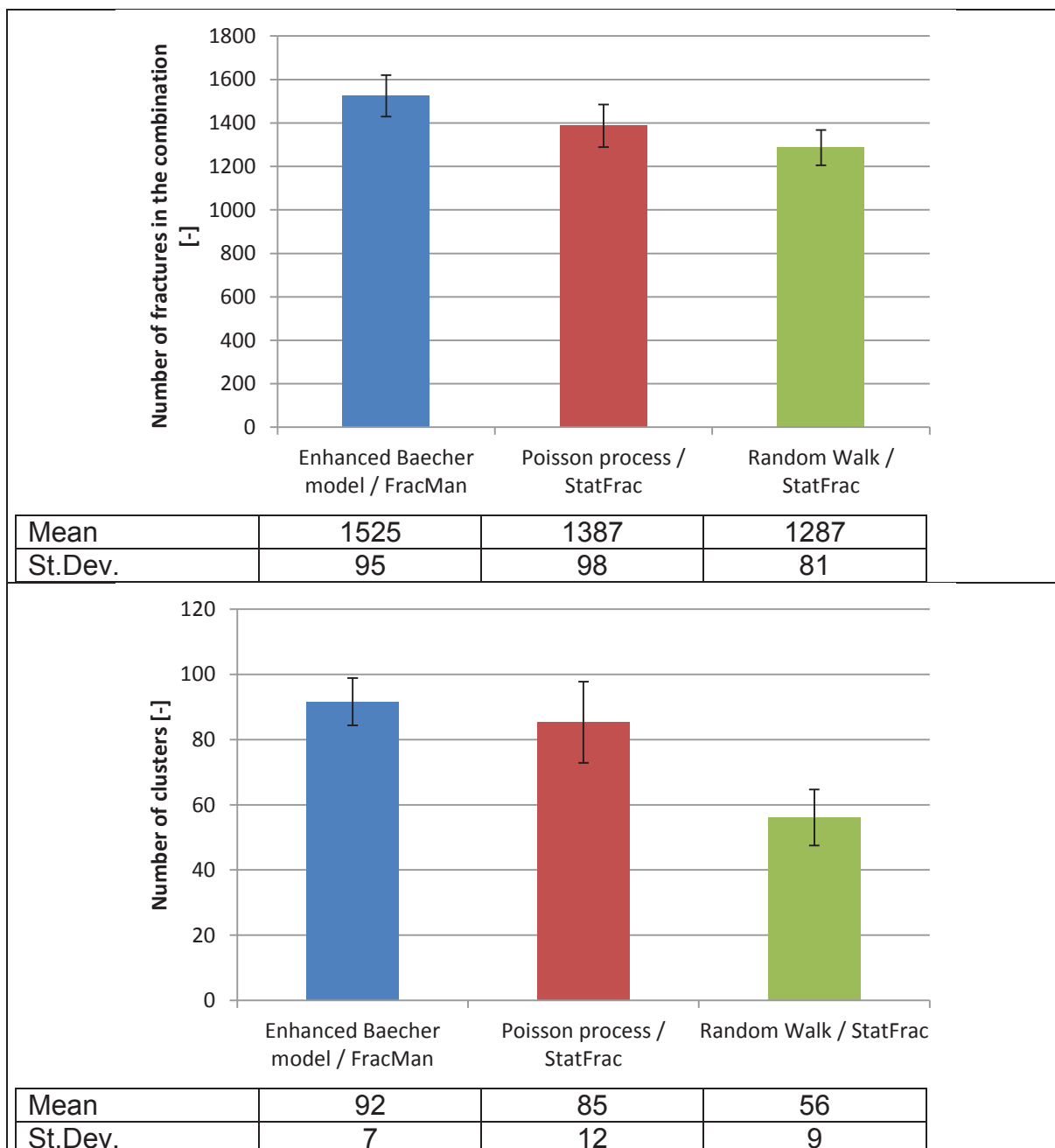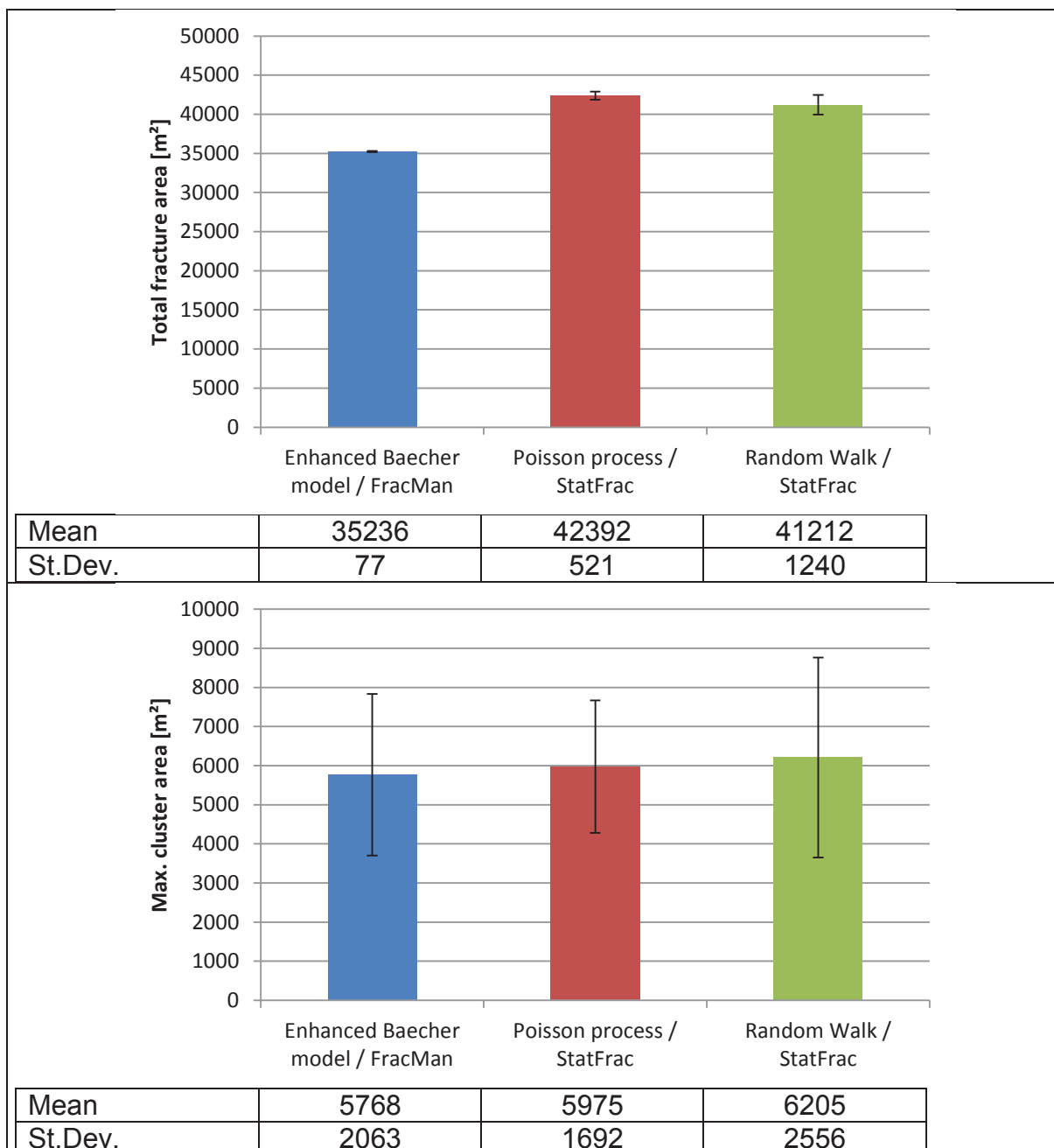
Figure 21. Cluster statistics including error bars

	Enhanced Baecher model / FracMan	Poisson process / StatFrac	Random Walk / StatFrac
Mean	35236	42392	41212
St.Dev.	77	521	1240

	Enhanced Baecher model / FracMan	Poisson process / StatFrac	Random Walk / StatFrac
Mean	5768	5975	6205
St.Dev.	2063	1692	2556

The number of fractures generated with the different algorithms does not show huge differences. Contrary to the number of clusters within the combination, while FracMan generates the most clusters, which is not necessarily good as it seems that there are many small ones, StatFrac generates less. It seems that FracMan generates much more small fractures than both algorithms in StatFrac and that there are a lot of tiny clusters as the fracture area is about 16% less.

The highest range of results was achieved with the maximum fracture area. The biggest cluster in FracMan models ranges between 3876 and 11102 m², StatFrac using the poisson process it ranges between 3522 and 8032 m² and using the random walk the range is between 3538 and 12979 m².

5.3 Flow data analysis

In this section the results from flow data analysis are shown. I start in showing the results from a single model and proceed in presenting results for 10 equi-probable DFM models while also varying the rock matrix permeability. All models have been generated using the Poisson process (StatFrac) as a stochastic generation algorithm. The model edge length is 50 meters and the combinations consist out of 4 fracture sets with an average of 1387 fractures with a standard deviation of 98.

In Table 6 the results for $k_{equ.}$ and q_f/q_m for one DFM realisation are shown. The output from the $k_{equ.}$- q_f/q_m tool used in flow based upscaling not just gives the overall equivalent permeability and fracture matrix flow, it is possible divide the results for the different flow directions (x,y,z) to see the impact of fracture orientation of the different fracture sets. Fracture sets oriented in flow direction have a higher impact, than sets oriented more perpendicular. This effect is visible in the difference of the results for the different flow directions x,y and z.

$k_{equ.}$ [mD]		q_f/q_m [-]	
k_x[mD]	57	$q_f/q_{m\ x}$[-]	112
k_y[mD]	761	$q_f/q_{m\ y}$ [-]	1502
k_z [mD]	319	$q_f/q_{m\ z}$ [-]	630

Table 6. $k_{equ.}$ and q_f/q_m results for one DFM model

To see the effect of matrix permeability on equivalent permeability and fracture – matrix flow (qf/qm), I repeated the simulation for ten equi-probable models, while varying matrix permeability (km=5 mD; km=5 mD, km=50 mD). Another aspect was to get an idea of the uncertainty according to the influence of the equi- probable models. Figure 22 shows the results for equivalent permeability using the average of the ten equi-probable models.
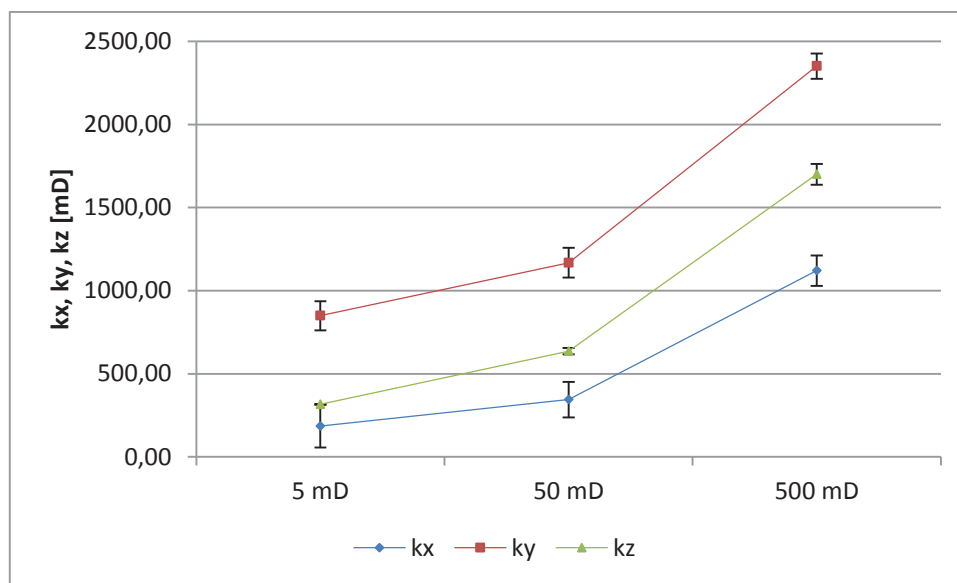
Figure 22. Matrix permeability variation – results for equivalent permeability

The influence of matrix permeability is clearly visible due to the increase of kx, ky and kz with increasing matrix permeability. The uncertainty in percent is summarized in Table 7. Uncertainty decreases with increasing matrix permeability, except for z direction, here it increases. As fracture sets which are oriented in flow direction have a higher impact than the sets oriented more perpendicular, also a difference between bottom-top (ky), left-right (kx) and front – back (kz) was achieved. Due to orientation of the fracture sets, best results have been achieved with a flow from bottom to top (ky) of the box, followed by front to back (kz) of the model. This might mean that the better the fractures are oriented regarding to flow direction the lower the permeability difference between the different equi-probable models gets.

used km	uncertainty kx	uncertainty ky	uncertainty kz
5 mD	69 %	10 %	1 %
50 mD	31 %	8 %	3 %
500 mD	8 %	3 %	4 %

Table 7. Uncertainty of kx, ky and kz in %

Figure 23 shows the results for fracture matrix flow. The lower km. the higher qf/qm. As kequ. rises with increasing rock matrix permeability, qf/qm decreases due to the high influence of matrix permeability. The uncertainty in percent (Table 7) is equal to the results for kx, ky and kz.
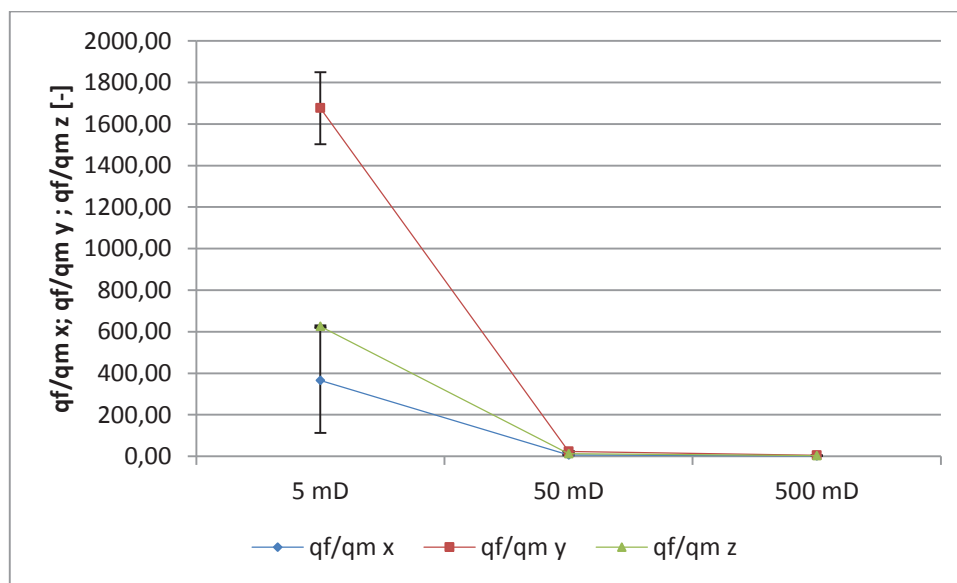
Figure 23. Matrix permeability variation – Results for qf/qm

Figure 24 shows an example for volume flux generated in StatFrac with the Poisson process using a rock matrix permeability of 5 mD. The two models with the highest differences in kx, ky and kz are shown. Best volume flux results are achieved in direction with the highest permeability, namely ky.

Figure 24 shows the flow velocity spectra for x, y and z direction separately for all four fracture sets and the flow velocity spectra for the combined fracture sets in the DFM model. The two models with the highest differences have been opposed in Figure 24.

y-DIRECTION

Fracture Set 1

Fracture Set 2

Fracture Set 3

Fracture Set 4

z- DIRECTION

Fracture Set 1

Fracture Set 2

normalized volume [-] | log velocity [m/s]

normalized volume [-] | log velocity [m/s]

Fracture Set 3

normalized volume [-] | log velocity [m/s]

normalized volume [-] | log velocity [m/s]

Fracture Set 4

normalized volume [-] | log velocity [m/s]

normalized volume [-] | log velocity [m/s]

ALL FRACTURES

x

normalized volume [-] | log velocity [m/s]

normalized volume [-] | log velocity [m/s]

y

normalized volume [-] | log velocity [m/s]

normalized volume [-] | log velocity [m/s]

Figure 24. Flow velocity spectra

Table 8 summarizes the mean and the standard deviation of the flow velocity spectra.

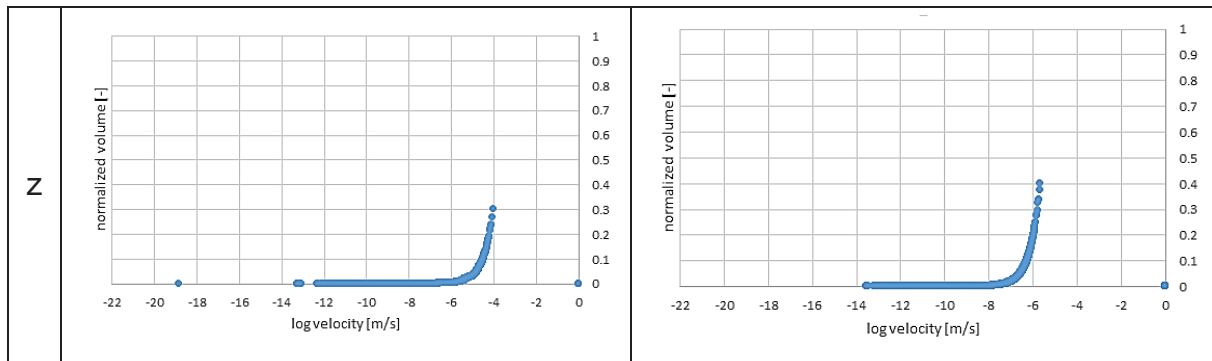|	Fracture set 1		Fracture set 2	
	Model 1	Model 2	Model 1	Model 2
x	$\pm$ -5.15 (-5.10)	$\pm$ -5.14 (-4.96)	$\pm$ -5.28 (-5.15)	$\pm$ -5.16 (-5.02)
y	$\pm$ -6.04 (-5.75)	$\pm$ -5.59 (-5.33)	$\pm$ -5.90 (-5.60)	$\pm$ -5.62 (-5.35)
z	$\pm$ -5.39 (-5.20)	$\pm$ -5.50 (-5.37)	$\pm$ -5.73 (-5.45)	$\pm$ -5.49 (-5.27)
	Fracture set 4		**Fracture set 3**	
	Model 1	Model 2	Model 1	Model 2
x	$\pm$ -5.18 (-5.04)	$\pm$ -5.09 (-4.98)	$\pm$ -5.20 (-5.19)	$\pm$ -5.29 (-5.05)
y	$\pm$ -6.27 (-5.89)	$\pm$ -5.18 (-5.05)	$\pm$ -5.96 (-5.75)	$\pm$ -5.61 (-5.40)
z	$\pm$ -5.50 (-5.26)	$\pm$ -5.49 (-5.29)	$\pm$ -5.58 (-5.37)	$\pm$ -5.71 (-5.32)
	All fracture sets			
	Model 1		Model 2	
x	$\pm$ -6.02 (-5.72)		$\pm$ -5.46 (-5.21)	
y	$\pm$ -6.27 (-5.89)		$\pm$ -6.05 (-5.63)	
z	$\pm$ -5.53 (-5.30)		$\pm$ -5.17 (-5.00)	

Table 8. Mean and standard deviation of the flow velocity spectra

The results in Figure 25 show, that the lowest difference is achieved for z direction and the highest for y direction. This leads me to the assumption that the fractures which are oriented to flow direction have the highest impact on flow and in this direction the lowest difference between the models is achieved.
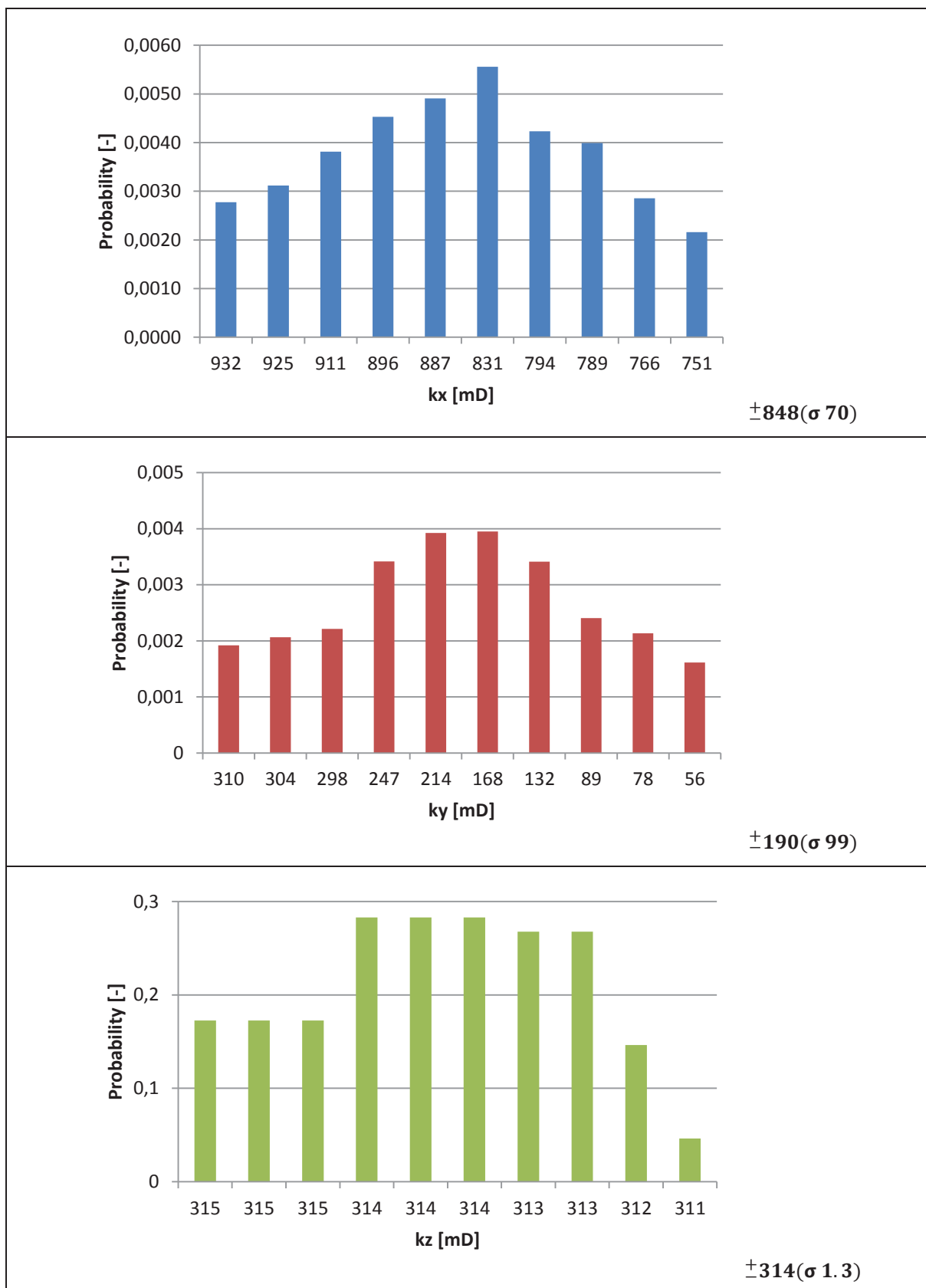
Figure 25. Probability distribution for k_equ. for 10 equi-probable models

6. Discussion

This master thesis has investigated the importance of a statistical analysis of stochastically generated DFM models. The purpose of this thesis was to determine the uncertainty concerning fracture generation algorithms used, model size, stochastically generated fracture geometries, variation of the size of the clusters within stochastically generated DFM models and the effect on variability of the kequ. and the qf/qm ratio.

One of the major findings concerning the generated fracture geometries using different fracture generation algorithms is that the accuracy of the input vs. the output value of P32 not just depends on model size but also on the fracture generation algorithm used. While the uncertainty of the Poisson process and the Random walk used in StatFrac was about 25% for the smallest model size, the Enhanced Baecher model had an uncertainty of 97%. This high uncertainty would have an immense effect on the reliability of the DFM model. I assume that the fracture generation algorithm has even a higher influence on the uncertainty than the used model size, even if P32 gets more accurate with an increase in model size. Results with an uncertainty below 5 % have been achieved with an increase in model size.

Next, the used cut-off for the power law fracture length distribution need to be discussed. The minimum cut-off value defines the smallest fractures included in the model and determines how complex the model and so the mesh gets. Setting the minimum cut off value too high would lead to a truncation effect (Bonnet, et al., 2001). This influences the validity of the input statistics. Using a minimum cut off- value of 0.5 meter for the fracture radii, fracture generation algorithms used in StatFrac produce a power law distribution. In FracMan the "clipping" process changes the input distribution

(PL) to a log-normal distribution. This occurs because fracture centres are not necessarily set in the model domain, this could destroy the input statistics. Another point is that FracMan produces a higher amount of small fractures to reach P32 and so less big fractures than fracture generation algorithms in StatFrac. I assume that StatFrac this higher amount of "big" fractures (10-27.4 meter) is an effect of the forbidden zones included, as the smaller fracture will be deleted if it would be set in the forbidden zone. An interesting finding is, that the maximum fracture radius had an uncertainty below 10% for all fracture generation models. For models with a model edge length higher than 25 meter it was even below 1%.

But in fact, not just the size of the fractures has an impact on flow, but also the location within the box volume. The aim would be that the cluster spans the entire region to reach a percolation threshold. Odling et al. (1999) also described the relationship between fracture density and number of fractures within a cluster. So with a small fracture density also the clusters themselves are smaller, which leads to the result that no cluster spans the entire region. As I used a power law relationship more small fractures have been generated in the model than big ones. I assume that even with a high fracture density a high variation of results concerning percolation threshold will be achieved. Due to this I was interested in the biggest cluster of the equi-probable models. On the question of the variation of the biggest cluster, this study found that there is a high diversity of the results, e.g. the maximum cluster area generated with the Poisson process in StatFrac is $\pm$5975 (3384) m². Surprisingly about the same amount of fractures (~ 30%) are interconnected in every model and all three fracture generation algorithms produced about the same amount of the total number of fractures in the model (Enhanced Baecher: $\pm$ 1525 (190); Poisson Process $\pm$ 1387

(196); Random Walk $\pm$ 1287 (162)). So I assume the location in the box volume has the highest influence on the biggest cluster. But also here the fracture generation algorithm has an influence, as in models generated with the Enhanced Baecher algorithm a higher amount of clusters exist, but within these are lots of small clusters, which have little effect on percolation.

Next, I want to discuss the uncertainty in flow data analysis. Ahmed Elfeel and Geiger (2012) listed the high dependency on boundary conditions as a negative aspect of flow based upscaling. I conclude that the results are sensitive to different boundary conditions and different uncertainties might occur than in my study.

The uncertainty analysis for the equivalent permeability divided in x, y and z direction has shown that fractures which are oriented to flow direction have not just the highest impact on flow but also the lowest uncertainty between the models is achieved. The highest uncertainty was found in x direction, due to the orientation of the fractures. Another factor which influences uncertainty is the rock matrix permeability, as higher matrix permeability leads to a lower uncertainty. Also for fracture matrix flow similar results have been achieved. A higher influence of the rock matrix leaded to a lower uncertainty in the results (below 10% for km=500 mD).

These findings are significant, as I've shown that the stochastically generation of DFM models can lead to a not neglible uncertainty with regard to kequ. and qf/qm.

7. Conclusions

How much do multiple realisations differ from one another? How much does the variability among the stochastically generated DFMs affect $k_{equ.}$ qf/qm, the size of percolating clusters and the flow velocity spectra? The aim of my thesis was to answer these questions. The major findings of this study are listed below:

- The accuracy of P32 not just depends on the model size, but even more on the fracture generation algorithm used. I conclude that fracture generation algorithms which consider forbidden zones lead to a lower uncertainty.

- The clipping process used in FracMan might destroy fracture input statistics. In this study a fracture length power law distribution became log-normal.

- More small fractures are generated with the Enhanced Baecher model in FracMan than with StatFrac generation algorithms. This again results from the included forbidden zones and might affect the percolation threshold.

- The input vs output maximum fracture radius reveals to a low uncertainty for all fracture generation algorithms. But also here, a bigger model size leads to an increase in accuracy.

- The location of the fractures in the box volume has a very high influence on the biggest cluster and its fracture area. Here the highest uncertainty occurs, with a high diversity in results, this has a high influence on percolation threshold.

- The highest uncertainty for kequ. and qf/qm occurs in direction where most fractures are oriented perpendicular to flow direction. Another influence on equivalent permeability and fracture matrix flow has the rock matrix permeability. A higher rock matrix permeability leads to a lower uncertainty.

Taken together, these findings show that uncertainty has to be considered in DFM model generation.

8. References

Adler, P. & Thovert, J.-F., 1999. Theory and applications of transport in porous media. In: K. A. Publishers, ed. *Fractures and Fracture Network.* Netherlands: s.n., pp. 6-8.
Ahmed Elfeel, M. & Geiger, S., 2012. Static and Dynamic Assessment of DFN Permeability Upscaling. Volume SPE 154369.

Bogdanov, I., Mourzenko, V., Thovert, J.-F. & Adler, P., 2007. Effective permeability of fractured porous media with power-law distribution of fracture sizes. *Physical Review E., Statistical, nonlinear, and soft matter physics*, September.

Bonnet, E. et al., 2001. Scaling of fracture systems in geological media. *Reviews of Geophysics,* Volume 39, pp. 347-383.

Cooper, S., 2000. *Deformation within a basement-cored anticline, Teapot Dome Wyoming,* Socorro, New Mexico: Department of Earth and Environmental Science.

Cooper, S. & Lorenz, J., 2001. *Lithologic and Structural Controls on Natural Fracture Characteristics Teapot Dome, Wyoming,* Sandia National Laboratories: Geophysical Technology Department.

Dershowitz, W., 1992. *Interpretation of fracture spacing and intensity,* Rotterdam: Rock Mechanics, Tillerson & Wawersik.

Dietrich, P. et al., 2005. *Flow and Transport in Fractured Porous Media.* s.l.:Springer Verlag Berlin Heidelberg.

Gudmundsson, A., 2011. *Rock Fractures in Geological Processes.* s.l.:Cambridge University Press.

Inc., G., 2012. *earth.google.com.* [Online].

Lato, M., Diederichs, M. & Hutchinson, D., 2010. Bias Correction for View-limited Lidar Scanning of Rock Outcrops for Structural Characterisation. In: S. Verlag, ed. s.l.:Rock Mech Rock Eng.

Matthäi, S., 2012. *Apart from mechanical fracture aperture: What can we do better?.* itf-ISF3 meeting Scotland, s.n.

Matthäi, S. & Belayneh, M., 2004. *'Fluid flow partitioning between fractures and permeable rock matrix,* s.l.: Geophysical Research Letters, Vol. 31.

Matthäi, S. & Nick, H., 2009. Upscaling two-phase flow in naturally fractured reservoirs. *AAPG Bulletin,* 93(11), pp. 1621-1632.

Min, K.-B., Jing, L. & Stephansson, O., 2004. Determining the equivalent permeability tensor for fractured rock masses using a stochastic REV approach: Method and application to the field data from Sellafield, UK. *Hydrogeology Journal,* Volume 12, pp. 497-510.

Odling, N. et al., 1999. Variation in fracture system geometry and their implications for fluid flow in fractures hydrocarbon reservoirs. *Petroleum Geoscience Vol. 5*, pp. 373 - 384.

Ouenes, A. et al., 2010. *Integrated Characterisation and Simulation of the Fractured Tensleep Reservoir at Teapot Dome for CO2 Injection Design,* California: SPE 132404.

Pollard, D. & Aydin, A., 2007. *Progress in Understanding Jointing over the Past Century.*[Online] Available at: http://pangea.stanford.edu/~zhongj/articleS/atc/a1.htm [Accessed June 2007].

Sangare, D., Thovert, J.-F. & Adler, P., 2010. Macroscopic properties of fractured porous media. *Physica A Statistical Mechanics and its Applications*, March, p. Vol. 389; No. 5.

Schwartz, B., 2006. *Fracture Pattern of Tensleep Formation,* West Virginia: Department of Geology and Geography.

Smith, V., 2012. *Modeling Natural Fractured Networks: Establishing the Groundwork for flow simulation at Teapot Dome Wyoming.* West Virginia: Proquest, Umi Dissertation Publishing.

Snow, D., 1969. Anisotropic Permeability of Fractured Media. *Water Resources Research,* Vol. 5(No.6), pp. 1273-1289.

Wilson, C. & Witherspoon, P., 1974. Steady state flow in rigid networks of fractures. *Water Resources Research,* Volume 10, pp. 328-335.

Wilson, T., Smith, V. & Brown, A., 2013. *Characterization of Tensleep Reservoir Fracture Systems Using Outcrop Analog, Fracture Image Logs and 3D Seismic,* s.l.: Search and Discovery Article #50877.

Yin, P., 2005. *Characterisation of Tensleep Reservoirs,* University Wyoming: Enhanced Oil Recovery Institute.

Appendix A.

The phyton script for the cluster count is shown here. The coordinates, the radius and the orientation of the fractures are used to locate the fractures and to check if they are interconnected with other fractures. The script finishes with an output of the number of clusters in the model, the number of fractures in a cluster and the total fracture area of a cluster.

```python
import shlex
import Utilities
import Rhino.Geometry
import itertools
import math

def readFromFiles():
    fraclist = []
    height = 0.0001
    files = ["Fracture_Half_Lengths_set1_1","Fracture_Half_Lengths_set2_1",
"Fracture_Half_Lengths_set3_1","Fracture_Half_Lengths_set4_1"]
    for file in files:
        print "open file", file
        f = open(file, "r")
        lines = f.readlines()
        for l in lines:
            [x, y, z, radius, dip, dipangle] = shlex.split(l)
            flaw = Rhino.Geometry.Point3d(float(x), float(y), float(z))
            vec = Utilities.CreateOrientationVector(float(dip), float(dipangle))
            plane = Rhino.Geometry.Plane(flaw, vec)
            circle = Rhino.Geometry.Circle(plane, float(radius))
            cylinder = Rhino.Geometry.Cylinder (circle, height).ToBrep(True, True)
            fracture = [0, cylinder, radius]
            fraclist.append(fracture)
    return fraclist

def countClusters(fraclist):
    clusterCount = 1
    checklist = list(itertools.combinations(fraclist, 2))
    for pair in checklist:
        intersection      =      Rhino.Geometry.Intersect.Intersection.BrepBrep(pair[0][1],
pair[1][1], Rhino.RhinoMath.SqrtEpsilon)
        if len(intersection[1]) != 0:
            if (not pair[0][0]) and (not pair[1][0]):
                pair[0][0] = clusterCount
                pair[1][0] = clusterCount
                clusterCount = clusterCount + 1
```

```python
            else:
                if pair[0][0] > pair[1][0]:
                    pair[1][0] = pair[0][0]
                    if pair[1][0]:
                        for frac in fraclist:
                            if frac[0] == pair[1][0]:
                                frac[0] = pair[0][0]
                else:
                    pair[0][0] = pair[1][0]
                    if pair[0][0]:
                        for frac in fraclist:
                            if frac[0] == pair[0][0]:
                                frac[0] = pair[1][0]
    clusterCount = clusterCount - 1
    for frac in fraclist:
        print frac[0]
    f = open("cluster_analysis.txt", "w")
    f.write("Number of Clusters\t" + str(clusterCount) + "\n")
    count = []
    area = []
    for i in xrange (clusterCount):
        count.append(0)
        area.append(0.)
        for frac in fraclist:
            if frac[0] == i+1:
                count[i] = count[i] + 1
                S = math.pi*float(frac[2])*float(frac[2])
                area[i] = float(area[i]) + float(S)
        f.write(str(i+1) + "\t" + str(count[i]) + "\t" + str(area[i]) + "\n")
    f.close()
    print "Done"


def main_function():
    fraclist = []
    fraclist = readFromFiles()
    countClusters(fraclist)


if( __name__ == "__main__" ):
    main_function()
```